JGS
Journal of the Geological Society

Research article

Published online July 30, 2018 https://doi.org/10.1144/jgs2017-117 | Vol. 175 | 2018 | pp. 820–835

# Thermal evolution in the exhumed basement of a stratovolcano: case study of the Miocene Mátra Volcano, Pannonian Basin


**Róbert Arató[1,2,3], István Dunkl[2], Ágnes Takács[1], Géza Szebényi[4], Axel Gerdes[5] & Hilmar von Eynatten[2]**

[1] Department of Mineralogy, Eötvös Loránd University, Pázmány Péter sétány 1/C, H-1117 Budapest, Hungary
[2] Geoscience Centre, Sedimentology and Environmental Geology, University of Göttingen, Goldschmidtstrasse 3, D-37077 Göttingen, Germany
[3] Present address: Hungarian Academy of Sciences, Institute for Nuclear Research, Bem tér 18/C, H-4026 Debrecen, Hungary
[4] Mecsekérc Zrt., Esztergár Lajos utca 19, H-7633 Pécs, Hungary
[5] Department of Geosciences, Goethe University Frankfurt, 60438 Frankfurt am Main, Germany
R.A., 0000-0002-9983-6435
* Correspondence: arato.robert@atomki.mta.hu

**Abstract:** The thermal influence of a Miocene stratovolcano (Mátra Volcano) on its basement was studied by apatite and zircon (U–Th)/He thermochronometry. The pre-Miocene substratum of the volcano contains Mesozoic sedimentary units in addition to the nearby exhumed igneous Recsk Complex. The Oligocene emplacement age of the Recsk Complex is constrained by zircon U–Pb geochronology to be 29.6 Ma, which serves as a benchmark for the beginning of its thermal history. All measured apatite (U–Th)/He ages (19.9–5.9 Ma) and most of the zircon (U–Th)/He ages (26.2–17.7 Ma) are considerably younger than the emplacement age of the Oligocene Recsk Complex, implying thermal overprinting by the adjacent Miocene Mátra Volcano. The apatite and zircon He ages of the Oligocene complex increase from south to north, providing clear evidence of a northwards-weakening thermal overprint. The post-Oligocene thermal history of the basement was reconstructed via one-dimensional subsidence/thermal modelling. According to zircon He modelling, the thickness of the covering units above the Recsk Complex was estimated to be 1000–1500 m and the heat flux was *c.* 200 mW $m^{-2}$ during the Miocene volcanism. Thermal modelling based on apatite He data suggests that the Miocene volcanism was followed by intensive erosion and the exposure of the Recsk Complex by the Late Miocene.

**Supplementary material:** The locality, petrography and age yield of the dated samples of the Recsk Igneous Complex and details of the laser ablation inductively coupled plasma mass spectrometry dating of zircons from the Recsk Complex are available at: https://doi.org/10.6084/m9.figshare.c.4127444

**Received** 3 October 2017; **revised** 30 May 2018; **accepted** 6 June 2018

The Recsk Complex is the most northeasterly member of the Paleogene Periadriatic magmatic suite, which ranges from the westernmost Southern Alps to the northern Pannonian Basin (Fig. 1). This *c.* 900 km long igneous belt consists of numerous calc-alkaline, subduction-related intrusive bodies arranged along the Periadriatic Lineament (e.g. Bergomi *et al.* 2015). In the eastern section of the belt, mainly in the Pannonian Basin, the stratovolcanic edifices are also well preserved (e.g. Benedek 2002). In some volcanic centres and igneous stocks the magmatism was followed by the formation of various ore bodies, e.g. porphyry, skarn and epithermal ore mineralization. The Recsk Igneous Complex hosts one of the largest porphyry–skarn–epithermal deposits in the Alpine–Carpathian region. Its porphyry Cu–(Mo–Au) and Cu–Zn(–Fe) skarn ore deposits have been explored by a total of 156 000 m of surface diamond drillings and by two 1200 m deep shafts (Földessy & Szebényi 2008), which provide an excellent three-dimensional database of the area.

The Oligocene Recsk Complex is uniquely situated at the intersection of the Paleogene Periadriatic igneous belt and the Miocene–Quaternary calc-alkaline volcanic belt of the Carpathian arc (Fig. 1) in the immediate vicinity of the Miocene Mátra Volcano (Fig. 2). We assume that the Mátra Volcano covered a much larger area in the Miocene than today – during and after its active period – and that it thermally influenced its basement, including the Recsk Complex. The Oligocene zircon U–Pb ages of this study set the time benchmark for the beginning of the thermal evolution of the Recsk Complex. To constrain the post-emplacement thermal history, we applied apatite and zircon (U–Th)/He thermochronology (AHe and ZHe, respectively) to the volcanic, volcanoclastic and intrusive rocks of the Recsk Complex and one Miocene tuff. The closure temperatures of these thermochronometers are *c.* 60°C for AHe and between 130 and 180°C for ZHe (e.g. Farley 2002; Reiners *et al.* 2004), so they are sensitive to shallow crustal thermal events. The sampling was performed in a three-dimensional network covering >1200 m vertical and *c.* 8500 m horizontal distance between the samples. Apart from the mineralized zones, the sample material is well suited for thermochronology because the individual units of the Recsk Complex contain well-developed and inclusion-free/-poor accessory minerals.

As a result of the exhumation and preservation of the Oligocene intrusive and volcanic formations (Recsk), the thermal evolution in the basement of a younger Miocene volcano (Mátra) could be uniquely well studied. Therefore this work serves as a case study for describing and quantifying the thermal evolution below a stratovolcanic edifice. The reconstruction of the thermal history at different parts of the Recsk Complex is primarily based on the robust thermochronological data of the current study. The thermal/subsidence modelling is based on fixed values (e.g. geological facts, such as the thickness of the sedimentary cover preserved below the Miocene volcanic edifice) and on variable parameters, such as the palaeoheat flux and the thickness of the eroded volcanic cover sequence. The reliability of the assumed parameters and the

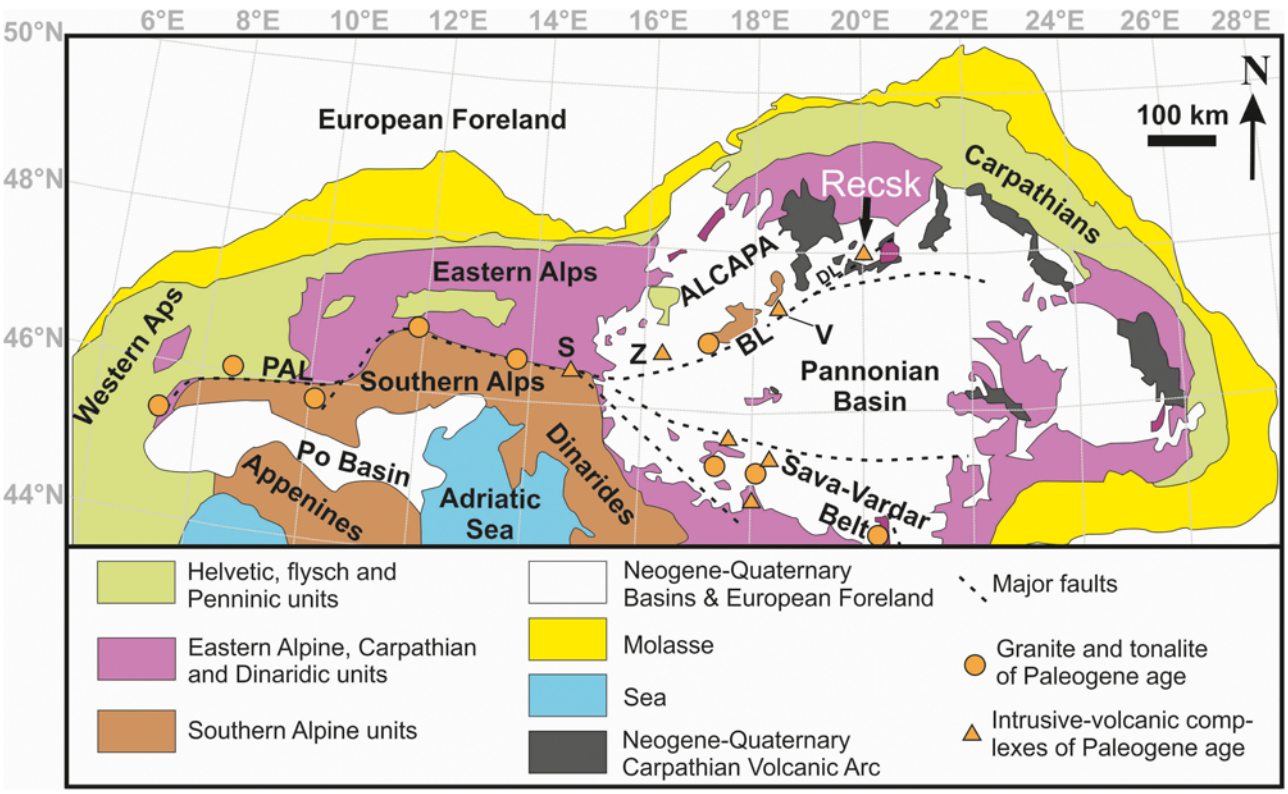


**Fig. 1.** Overview of the Paleogene calc-alkaline magmatic centres along the Periadriatic Lineament and the Balaton Line. Map base after Molnár *et al.* (2008), with simplifications. ALCAPA, Alpine-Carpathian-Pannonian tectonic unit; BL, Balaton Line; DL, Darnó Line; PAL, Periadriatic Lineament; S, Smrekovec; V, Velence; Z, Zala.

modelled thermal/subsidence histories are verified by comparing the measured AHe and ZHe ages with the ages calculated by modelling.

## Geological setting

The Paleogene magmatic intrusions of the Alps are located in a narrow belt immediately to the south and north of the Periadriatic Lineament (Exner 1976). These igneous rocks are mostly of tonalitic–granodioritic composition, although felsic and gabbroic intrusions, lamprophyres, basaltic dykes and leucogranite bodies also occur (Fig. 1). The U–Pb, Rb/Sr and Ar/Ar ages of the igneous bodies scatter between 42 and 28 Ma, but there was a pronounced maximum of magmatic activity between 32 and 29 Ma (von Blanckenburg & Davies 1995; see compilation in Rosenberg 2004 and Bergomi *et al.* 2015).

The medium- to high-K calc-alkaline Paleogene magmatic centres of the Pannonian Basin are arranged along the Balaton Line, a significant SW–NE-trending strike-slip fault system (Fig. 1). The age and geochemical characteristics of these igneous rocks have similarities with the intermediate intrusive bodies of the Alps and with the Sava-Vardar Paleogene igneous belt (Benedek 2002; Pamić *et al.* 2002; Schefer *et al.* 2011). As a result of the intensive post-Oligocene exhumation of the Alps, the Periadriatic magmatic centres were eroded to the depth of their batholitic intrusions. By contrast, the mostly stagnating or subsiding tectonic regime in the Pannonian Basin allowed the preservation of the volcanic edifices and related shallow-level epithermal and porphyry ore deposits (Molnár *et al.* 2008). The igneous rocks of the Zala Basin (Hungary) are completely covered by younger sediments, whereas the Smrekovec (Slovenia), Recsk and Velence (both Hungary) volcanic centres crop out on the surface (Fig. 1; Székyné 1957; Benedek 2002).

The outcrop of the Recsk Complex occupies an area of *c.* 30 km$^2$ (Fig. 2). The magmatic body is bounded by WNW–ESE-trending, as well as NW–SE-, east–west- and north–south-trending younger faults related to the NE-trending faults of the Darnó Line (Molnár *et al.* 2008), a larger scale fault system to the east of the Recsk Complex (Fig. 1). The volcanic sequences can be divided into four subunits (Földessy *et al.* 2008). The lowest unit consists of submarine pyroxene–amphibole andesite, intercalated with shallow marine marl layers. It is covered by subaerial and subaqueous, hydrothermally altered, ore-bearing biotite–amphibole andesite lava, agglomerates, volcanogenic breccias and pyroclastic sequences in the northern part of the area at Lahóca Hill, and a dacitic lava–tuff complex in the south. The youngest volcanic unit is represented by a fresh, hydrothermally unaltered biotite–amphibole andesite. The volcanic rocks are co-genetic with the diorite–porphyry and quartz diorite intrusions situated *c.* 250–400 m below the present day surface (Molnár *et al.* 2008). Despite the wide range of published K–Ar ages determined on variable bulk rock samples and hydrothermal mineral phases (37–21 Ma, see Fig. 3a), the laser ablation zircon U–Pb ages of this study indicate that they all formed in <1 myr at *c.* 29.6 Ma. The subdivision of the volcanic sequences is thus of no significance in the thermochronological reconstruction.

In the western part of the complex, the Mesozoic rocks beneath the stratovolcano are covered with angular unconformity by Late Eocene (Priabonian) carbonates. According to calcareous nannoplankton biostratigraphy, the marl directly underlying the Recsk andesite was deposited at the Eocene–Oligocene boundary (NP 21 zone). A similar nannoplankton zone was determined for some sedimentary intercalations of the lower part of the stratovolcanic andesite, although only in two sections of a single borehole (Less *et al.* 2008). The large foraminifera fauna of the sediments directly overlying the andesite indicate an early Chattian age for the cover sequence (i.e. <28.1 Ma).

A younger calc-alkaline volcanic belt – consisting of numerous andesitic, rhyolitic and dacitic volcanic centres – developed along the mountain range of the Carpathians from the Neogene to the Quaternary (e.g. Póka 1988; Szabó *et al.* 1992; Pécskay *et al.*

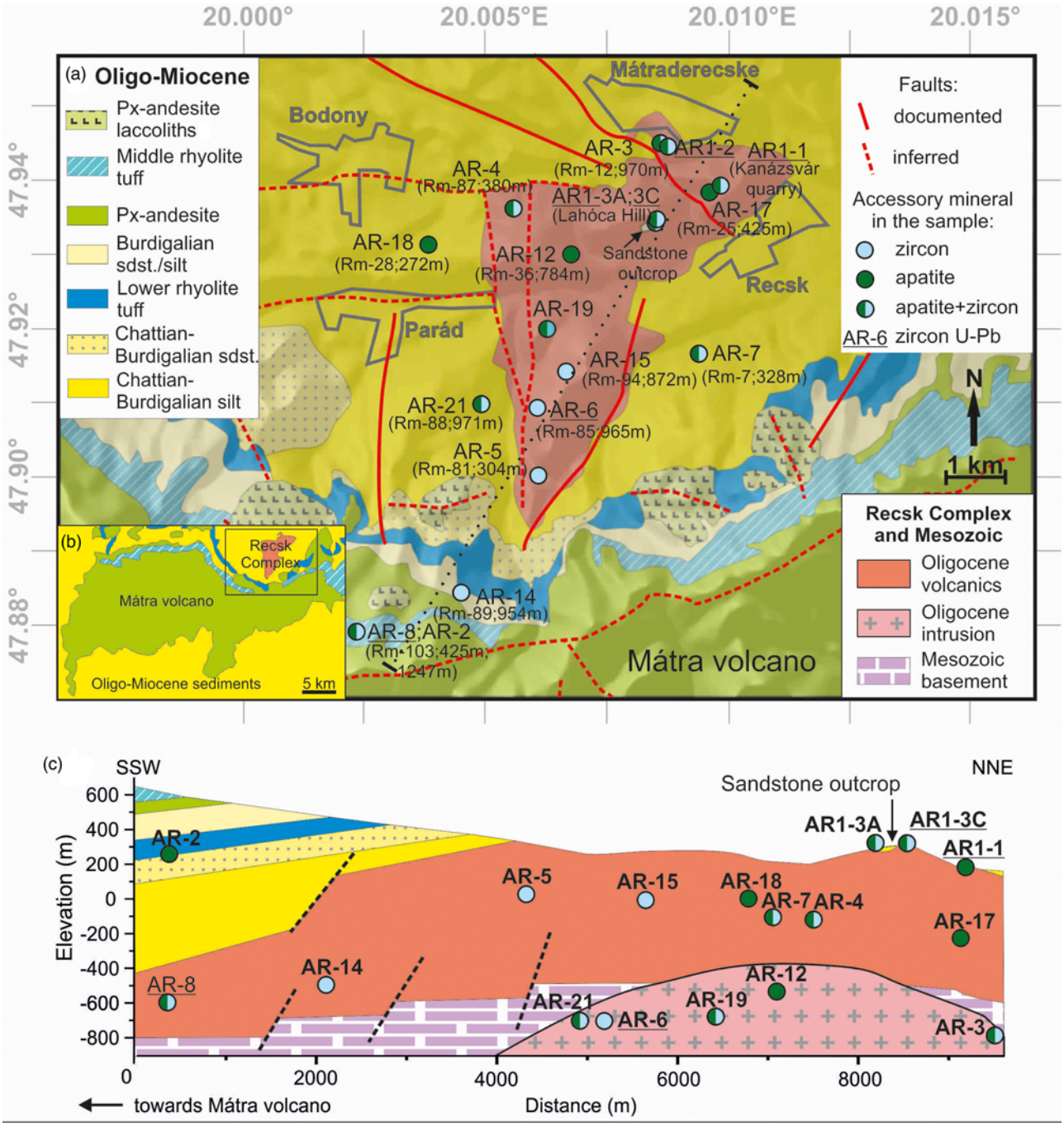


**Fig. 2.** (**a**) Pre-Quaternary geological map of the Oligocene Recsk Complex and the northeastern margin of the Miocene Mátra Volcano showing the sample sites (modified after Varga *et al.* 1975). The colour of the sample symbols indicates which mineral was available for low-temperature thermochronology. Rm numbers refer to the boreholes used for porphyry copper and polymetallic ore exploration. (**b**) Simplified pre-Quaternary geological map of the Mátra Volcano and the Recsk Complex. Map base after Gyalog (2013). The rectangle marks the position of map in part (a). (**c**) Slightly simplified SSW–NNE section across the Recsk Complex with sample codes; vertical exaggeration *c.* 2×; the trace of the section is indicated by the dotted line in part (a). Sample AR1-2 was only used for the U–Pb geochronology and is therefore not shown on the cross-section. px, pyroxene.

1995*a*, *b*; Harangi *et al.* 2006; Kovács *et al.* 2007; Kovács & Szabó 2008; Fig. 1). The stratovolcanic edifice of the Mátra Volcano consists of roughly three main andesitic units and three rhyolitic tuff horizons (Fig. 3). Andesites form the main mass of the volcano, with an overall thickness of a couple of 100 m to 2000 m. The whole-rock and biotite K–Ar ages of the main, and by far the most voluminous, andesitic sequence range between 16 and 13 Ma (Zelenka *et al.* 2004; Fig. 4a). This scatter, however, is more related to the bad Ar retentivity and high atmospheric Ar content of the dated phases than to the actual age range of andesite volcanism, which we assume to have been significantly shorter. The three tuff horizons are distributed over the entire Pannonian Basin and are used as marker horizons for the regional lithostratigraphy. The range of Miocene volcanism is benchmarked by the lowest rhyolite tuff (the K–Ar and U–Pb ages scatter between 18.2 and 17.1 Ma), whereas the youngest andesitic unit yielded ages from 12.5 to 11.8 Ma (Zelenka *et al.* 2004; Lukács *et al.* 2018). It remains a matter of debate whether the andesitic edifice forming the Mátra Mountains is only the remnant of a large caldera (Szádeczky-Kardoss 1958; Baksa *et al.* 1981) or whether it was formed by numerous, smaller eruption centres. The supporters of the single caldera hypothesis suggest that the Mátra Volcano used to be a 3000 m high volcano with a basal diameter of at least 13 km. Nonetheless, it is clear that the volcano was tilted to the south during Serravallian to Early Tortonian (Late Miocene) time because the

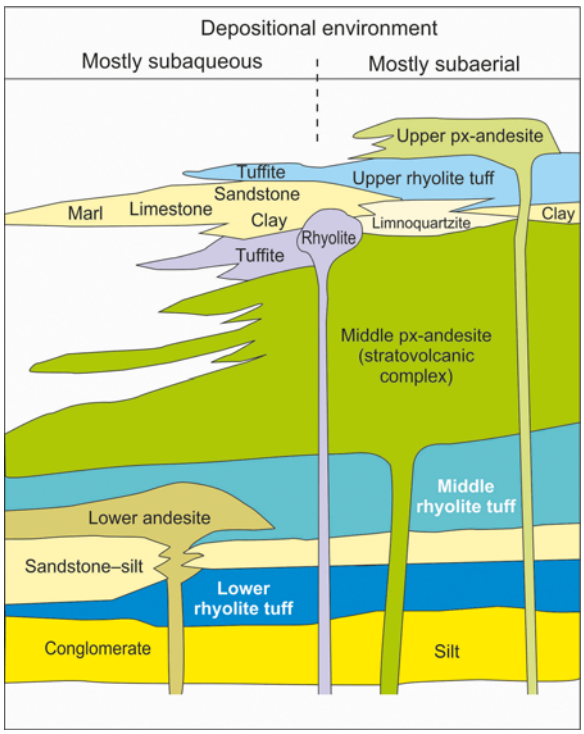


**Fig. 3.** Schematic stratigraphic column of Mátra Volcano. px, pyroxene.

boreholes south of the Mátra Mountains intersected the Serravallian, southward-dipping tuff horizon at a depth of 1500–1700 m b.s.l,; this tuff horizon is unconformably covered by horizontally deposited Tortonian sediments (Zelenka 2010). The same 'Middle rhyolite tuff' horizon can be found at the northern margin of the Mátra Mountains at *c.* 550–700 m a.s.l. (Fig. 2), however the angle of tilt is not straightforward to calculate because multiple faults can be found along the north–south transect of the Mátra Volcano.

## Samples and methods

### *Samples*

Twenty-nine samples were collected along a NNE–SSW-trending swath of the exposed Recsk Complex from both drill cores and surface outcrops (Fig. 2; see Supplementary material and Table EA1 for details on localities and petrography of the samples). The drill cores were taken from the collection of the Mining Museum at Recsk. As the study aimed to investigate the thermal effect of the Mátra Volcano, we selected samples from both the vicinity of the Mátra Volcano and from farther to the north. We sampled different volcanic and intrusive units at different depths to create a three-dimensional thermochronological dataset of the area. We tried to pick at least thumb-sized, preferably coarse-grained and unaltered rock pieces from the Recsk Complex and one sample from the cover sandstone. The sampling strategy aimed to represent the study area uniformly, but several samples had passed through hydrothermal alteration and did not contain enough suitable mineral grains for thermochronology. Therefore, especially the southern domains of the area remain underrepresented (Fig. 2).

### *Zircon U–Pb geochronology*

The samples were gently milled in a disc mill to fragments <500 μm in size and then sieved. The heavy minerals were concentrated using a shaking table and a solution of sodium polytungstate and then the

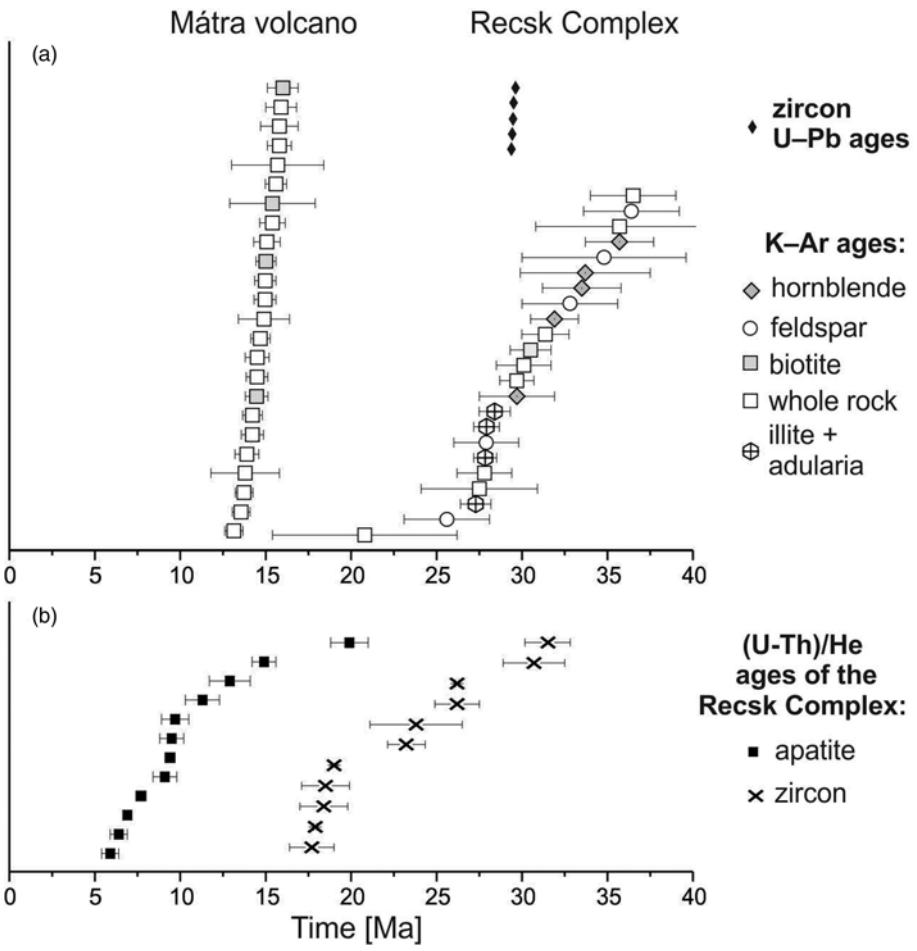


**Fig. 4.** (**a**) Compilation of geochronological data obtained on the Recsk Complex (illite and adularia K–Ar ages from Molnár *et al.* 2008; hornblende, feldspar, biotite and whole-rock K–Ar ages from Földessy *et al.* 2008; zircon U–Pb ages from this study) and the Miocene Mátra stratovolcano (Zelenka *et al.* 2004). (**b**) (U–Th)/He ages obtained in this study for the Recsk Complex.

low-susceptibility, U-bearing minerals were separated magnetically. Well-developed zircon crystals were hand-picked under a microscope and mounted in epoxy resin, followed by diamond polishing in five steps down to a diamond grain size of 1 μm. We obtained cathodoluminescence images for the properly exposed zircon grains using a JEOL JXA 8900 electron microprobe at the Geoscience Centre of the Georg August University, Göttingen. These images helped in studying the internal structure of the crystals and in the selection of homogeneous parts of the crystals for *in situ* geochronology. The zircon U–Pb measurements were carried out at the Institute of Geosciences, Goethe University Frankfurt using a Resonetics excimer laser ablation system coupled to an Element2 sector field inductively coupled plasma mass spectrometer (Košler & Sylvester 2003 ; Gehrels *et al.* 2008; Frei & Gerdes 2009). The age calculation was based on drift- and fractionation correction by standard sample bracketing using GJ-1 zircon reference material (Jackson *et al.* 2004). For further control, we analysed the Plešovice zircon (Sláma *et al.* 2008) and the 91500 zircon (Wiedenbeck *et al.* 1995) as secondary standards. The age results of the standards were consistent within $1\sigma$ of the published isotope dilution thermal ionization mass spectrometry values. The TuffZirc procedure (Ludwig 2012) was applied to identify the age of the youngest, most coherent, age component.

### *(U–Th)/He thermochronology*

The (U–Th)/He method is based on the measurement of the $^{4}$He that forms by the alpha decay of $^{238}$U, $^{235}$U, $^{232}$Th and $^{147}$Sm. As a result of this decay, in actinide- and Sm-bearing minerals (e.g. zircon, titanite and apatite), radiogenic He can accumulate on geological timescales. The main factors controlling the retention and diffusive loss of $^{4}$He are the crystal size, time and temperature (cooling/heating rate), the distribution of the parent isotopes and the density of radiation damage in the crystal lattice (Zeitler *et al.* 1987; Stockli *et al.* 2000; Farley 2002; Meesters & Dunai 2002*a*, *b*; Shuster *et al.* 2006; Herman *et al.* 2007; Flowers *et al.* 2007, 2009; Guenthner *et al.* 2013). $^{4}$He is partially retained in the He partial retention zone (PRZ), which is characteristic for each mineral (e.g. 40–80°C for apatite and 130–180°C for zircon), while almost total retention occurs below the so-called closure temperature (Dodson 1973; Farley 2002; Reiners *et al.* 2004). Depending on the thermal history of the rock, He ages can be interpreted as formation ages (e.g. volcanic eruptions), cooling ages (e.g. exhuming intrusions) or mixed ages (e.g. resulting from periods of burial heating with incomplete resetting in sedimentary basins and periods of exhumation; Wagner 1979).

The (U–Th)/He dating for this study was performed at the Geoscience Centre of the Georg August University, Göttingen. The apatite and zircon crystals were inspected for inclusions under 250× magnification and cross-polarized light. Only inclusion- and fissure-free, intact, euhedral grains >70 μm in width were selected. The shape parameters were determined and archived by multiple digital microphotographs. Single-crystal aliquots were dated, usually three to six aliquots per sample. The crystals were wrapped in Pt capsules of *c.* 1 × 1 mm size and heated by an infrared laser. The extracted gas was purified using an SAES Ti–Zr getter at 450°C. The chemically inert noble gases and a minor amount of other rest gases were then expanded into a Hiden triple-filter quadrupole mass spectrometer equipped with a positive ion counting detector. The crystals were checked for the degassing of He by sequential reheating and He measurements. The residual gas was usually *c.* 1–2% after the first extraction for zircon and always <1% for apatite. Following the degassing, the samples were retrieved from the gas extraction line and spiked with calibrated $^{230}$Th and $^{233}$U solutions. The zircon crystals were dissolved in pressurized Teflon bombs using a mixture of double-distilled 48% HF and 65% $HNO_3$ at 220°C for five days. The apatite crystals were dissolved in a 2% $HNO_3$ + 0.05% HF acid mixture in Savillex Teflon vials. Spiked solutions were analysed as 0.4 ml solutions via isotope dilution by a Perkin Elmer Elan DRC II inductively coupled plasma mass spectrometer with an APEX micro-flow nebulizer. The procedural U and Th blanks obtained by this method are usually very stable during a measurement session and <1.5 pg. Sm, Pt and Ca were determined by external calibration. The oxide formation rate and the PtAr–U interference was always monitored, but the effects of these isobaric argides were negligible relative to the signal of the actinides. The ejection correction factors ($F_t$) for single crystals were determined by the modified algorithm of Farley *et al.* (1996) using an in-house spreadsheet. The (U–Th)/He ages were calculated using Taylor series (McDougall & Harrison 1999).

## Results

### *Emplacement age of the Recsk Complex*

Table 1 summarizes the results of the zircon U–Pb geochronology and Table EA2 (Supplementary material) lists the raw laser ablation data. According to the cathodoluminescence imaging, the internal structure of the zircon crystals is dominated by regular oscillatory zoning and very few cores are present. The common Pb content is negligible (around the level of detection) in the majority of the dated zircons. The data are close to the concordia curve, thus the influence of inherited cores, common Pb, or Pb loss can be ruled out. We consider the ages determined by the TuffZirc procedure (Ludwig 2012) to represent the latest zircon growth period. Due to the small number of individual igneous bodies in the Recsk Complex, the residence time was probably short (Reid 2008), thus the zircon U–Pb ages are close to the age of the eruptions. U–Pb dating was performed on different units of the complex and the ages obtained were indistinguishable (Table 1). Thus the development of the entire volcanic edifice and subvolcanic intrusion(s) probably occurred within a few hundred thousand years at *c.* 29.6 Ma.

### *(U–Th)/He ages reflecting the post-emplacement thermal history*

The (U–Th)/He ages obtained on the Recsk Complex are presented in Table 2 and projected onto an SSW–NNE vertical section crossing the middle part of the igneous body (Fig. 5). The ZHe ages range from 31.5 to 17.7 Ma and yield two age groups: 31.5–23.1 Ma further to the north from the Mátra Volcano and 19.0–17.7 Ma in closer vicinity to the volcano in the south. The AHe ages range between 19.9 and 5.9 Ma (Fig. 4b) and are consistently younger than the ZHe ages measured in the same sample (Fig. 5). At a depth of 1000–1200 m below the surface, the ages scatter between 7.7 and 5.9 Ma, whereas at shallower depths (*c.* 300–400 m) they are slightly older (*c.* 11–9 Ma). Three surface samples in the northern part of the area yield 12.9 Ma (glauconitic sandstone), 14.9 Ma (fresh andesite) and 19.9 Ma (hydrothermally altered andesite).

We can assume that the Recsk Complex reached its post-Oligocene thermal maximum (i.e. maximum cover and heat flux) during the activity of the Mátra Volcano (*c.* 15 ± 1 Ma). Therefore He ages that are younger than 14 Ma can be considered to be completely reset (only AHe), whereas helium ages between 30 and 14 Ma are partially reset (AHe and ZHe). Judging from the measured ZHe ages, the Miocene Mátra volcanism and the post-Oligocene burial were unable to completely reset the ZHe thermochronometer. However, the lateral thermal influence of the Mátra Volcano is obvious from the northward increase in ZHe ages when comparing the data from the absolute elevation range of *c.* −500 to −800 m (Fig. 5). There is no detectable vertical gradient in the ZHe ages in the southern part of the Recsk Complex: the ZHe ages of group e range from 19.0 to 17.9 Ma,

**Table 1.** *Zircon U–Pb ages obtained on the different igneous units of the Recsk Complex. The sample means were calculated by the TuffZirc procedure (Ludwig 2012)*

| Sample no. | Location* | Lithology | Elevation (m a.s.l.)† | No. of crystals dated | No. of crystals considered by TuffZirc | U–Pb age (Ma) | 95% confidence errors + | – |
|---|---|---|---|---|---|---|---|---|
| AR-1-2 | Mátraderecske | Bedded tuff | +195 | 26 | 22 | 29.6 | 0.14 | 0.12 |
| AR-1-1 | Kanázsvár | Andesite | +221 | 28 | 26 | 29.5 | 0.09 | 0.10 |
| AR-1-3c | Lahóca | Andesite | +306 | 26 | 13 | 29.4 | 0.09 | 0.15 |
| AR-8 | Rm-103, 1247 m‡ | Quartz–biotite–amphibole andesite | −522 | 17 | 10 | 29.7 | 0.39 | 0.31 |
| AR-6 | Rm-85, 965 m‡ | Porphyritic diorite | −615 | 25 | 16 | 29.6 | 0.15 | 0.15 |

*Rm numbers refer to ore exploration boreholes.
†Negative values indicate depth below sea-level.
‡Borehole depth.

while sample AR-5 (situated *c.* 700 m higher than group e) yields a similar ZHe age (18.5 ± 1.4 Ma). By contrast, the AHe ages are all younger than the Oligocene emplacement age of the Recsk Complex and post-date the Miocene Mátra volcanism, except for two samples in the north (Fig. 5).

The measured (U–Th)/He ages are apparent ages that do not express a certain event, but result from a complex thermal history, including possible stagnation in the partial He retention zone. In order to define and quantify the main geological constraints that controlled the thermal history a thermal model was constructed, which is explained in detail in the next section.

To structure and simplify the dataset for modelling purposes, samples from similar depths with similar He ages were grouped as follows (Fig. 5, Table 3; Supplementary material, Table EA1).

(a) Apatite group a consists of surface samples from the north, representing a partially reset AHe age group (mean AHe age 14.2 ± 2.1 Ma). Note that the 19.9 Ma AHe age is not included in the group because the sample was collected from the hanging wall of a SW-verging reverse fault (Kupi 2006), clearly detected in the field between the AR1-3A and AR1-3C sampling sites.

(b) Apatite group b consists of shallow-seated andesitic samples at *c.* 300–400 m depth in the north, showing completely reset AHe ages between 11.4 and 9.1 Ma (mean AHe age 9.7 ± 1.5). Although in the same age range, sample AR-2 (11.3 Ma) from the south is not included because we expect that it had a different evolutionary history (heat flux and cover thickness), being formed in Miocene and positioned much closer to the Mátra Volcano.

(c) Apatite group c contains deep-seated andesitic–dioritic samples at uniform depth (*c.* 1000 m) in the north, showing completely reset AHe ages (mean AHe age 6.4 ± 1.0 Ma), which are, on average, younger than those of group b.

(d) Zircon group d consists of two shallow-seated (also included in group b) and one surface andesitic sample (also included in group a) in the northern segment of the Recsk Complex with a 29.5 ± 3.3 Ma mean ZHe age.

(e) Zircon group e represents the deep-seated ZHe group (mean ZHe age 18.3 ± 1.5 Ma) in the south at an average depth of *c.* 1000 m. There was not enough data to create more age groups in the southern segment of the Recsk Complex.

## Tandem modelling of the thermal and burial history

Our modelling procedure consists of two main steps. First, a one-dimensional transient heat flux was calculated based on a vertical crustal section consisting of layers (the Recsk Complex and its cover sequences) with different petrophysical properties. For this purpose, the PetroMod 1D software (Schlumberger) was used, which is a program routinely applied in the oil industry. It combines stratigraphic data, compaction and thermal conductivity trends of different lithologies, as well as geological knowledge, to model the thermal evolution and hydrocarbon potential of a sedimentary basin. The thermal evolution path calculated by PetroMod was used as input for the HeFTy software (Ketcham 2005), which computed the AHe and ZHe ages. These model ages were then compared with the measured thermochronological ages and their comparison was plotted by Surfer (Golden Software Inc.).

### *Constraints and parameters for modelling*

The Recsk Complex currently crops out at the surface. The reset apatite and zircon thermochronometers indicate an obvious post-Oligocene thermal overprint, meaning that the entire volume of the Recsk Complex experienced an increased palaeotemperature, which was significantly higher than its current temperature. The fairly well-known minor thickness of the Late Oligocene and post-Oligocene cover sediments of the region (500–1000 m; see Fig. 2) precludes the possibility that thermal blanketing through sedimentary burial alone resulted in this high palaeotemperature. The tilting of the Miocene strata, as well as the abrupt, steep and erosive northern termination of the Mátra volcanic sequence, point to a formerly wider extent. Therefore we assume that the Recsk Complex was covered by the northern extension of the Mátra stratovolcano. This burial, along with an increased heat flux during the active period of Miocene volcanism, must have been responsible for resetting the He thermochronometers. Consequently, the following post-emplacement processes were assumed to have controlled the thermal evolution of the Recsk Complex: (1) Oligo-Miocene sedimentation and related minor burial; (2) additional burial and increased heat flux related to the Miocene Mátra Volcano; and (3) the timing and rate of erosion of the cover sequences after the Miocene volcanism.

These geological processes were expressed numerically by five variable parameters: (1) the value of the increased Miocene heat flux triggered by the volcanism; (2) the duration of the increased heat flux; (3) the thickness of the Miocene volcanic cover; (4) the time when the erosion rate changed; and (5) the thickness of the remaining cover when the erosion rate had changed.

Parameters 4 and 5 serve to approximate an occasional non-uniform erosion and exhumation pattern after the peak of the Miocene volcanism, related to changes in regional tectonics such as the inversion of several parts of the Pannonian Basin after *c.* 10 Ma (Royden & Horváth 1988). All the variable parameters are shown graphically in Figure 6. Other input values of the modelling were kept constant based on either clear geological evidence or

**Table 2.** *Details of the apatite and zircon (U–Th)/He age results obtained for samples from the Recsk Igneous Complex*

| Sample | Aliquot | Crystal length (μm) | Prism length (μm) | Prism width (μm) | He | | $^{238}$U | | | $^{232}$Th | | | Th/U ratio | Sm | | | Ejection correction (Ft) | *Uncorrected He age (Ma)* | Ft-corrected He age (Ma) | 2σ (Ma) | Sample unweighted | |
|---|---|---|---|---|---|---|---|---|---|---|---|---|---|---|---|---|---|---|---|---|---|---|
| | | | | | Volume (ncc) | 1σ (%) | Mass (ng) | 1σ (%) | Concentration (ppm) | Mass (ng) | 1σ (%) | Concentration (ppm) | | Mass (ng) | 1σ (%) | Concentration (ppm) | | | | | mean ±2 SE (Ma) | |
| *Apatite (U–Th)/He ages* | | | | | | | | | | | | | | | | | | | | | | |
| AR-1-1 (R_4) | 1 | 179 | 131 | 85 | 0.112 | 2.0 | 0.048 | 2.3 | 17 | 0.116 | 2.5 | 42 | 2.42 | 0.35 | 6 | 125 | 0.68 | *11.8* | **17.2** | 1.9 | | |
| | 2 | 158 | 101 | 114 | 0.149 | 1.8 | 0.071 | 2.0 | 20 | 0.176 | 2.4 | 51 | 2.47 | 0.43 | 6 | 124 | 0.77 | *10.6* | **13.7** | 1.1 | | |
| | 3 | 142 | 113 | 73 | 0.098 | 2.0 | 0.044 | 2.3 | 19 | 0.119 | 2.5 | 52 | 2.72 | 0.27 | 8 | 119 | 0.63 | *11.0* | **17.5** | 2.2 | | |
| | 4 | 163 | 119 | 114 | 0.104 | 2.1 | 0.05 | 2.2 | 16 | 0.122 | 2.5 | 39 | 2.43 | 0.40 | 7 | 127 | 0.71 | *10.4* | **14.7** | 1.5 | | |
| | 5 | 231 | 137 | 125 | 0.275 | 1.5 | 0.124 | 1.9 | 15 | 0.342 | 2.4 | 42 | 2.75 | 0.94 | 6 | 117 | 0.78 | *10.7* | **13.7** | 1.1 | | |
| | 6 | 308 | 236 | 109 | 0.240 | 1.5 | 0.122 | 1.9 | 16 | 0.312 | 2.4 | 41 | 2.56 | 0.98 | 6 | 127 | 0.74 | *9.7* | **13.2** | 1.2 | | |
| | 7 | 209 | 171 | 140 | 0.333 | 1.4 | 0.144 | 1.9 | 17 | 0.37 | 2.4 | 43 | 2.56 | 1.00 | 6 | 118 | 0.80 | *11.5* | **14.3** | 1.0 | **14.9** | **0.7** |
| AR-1-3A | 1 | 263 | 191 | 100 | 0.201 | 1.7 | 0.104 | 1.9 | 17 | 0.261 | 2.4 | 43 | 2.51 | 0.75 | 6 | 124 | 0.82 | *9.7* | **11.8** | 0.8 | | |
| | 2 | 254 | 193 | 159 | 0.455 | 1.3 | 0.214 | 1.8 | 15 | 0.501 | 2.4 | 36 | 2.34 | 1.61 | 6 | 117 | 0.83 | *10.9* | **13.2** | 0.9 | | |
| | 3 | 160 | 114 | 114 | 0.463 | 1.1 | 0.213 | 1.8 | 20 | 0.390 | 2.4 | 36 | 1.83 | 1.36 | 6 | 127 | 0.75 | *12.1* | **16.1** | 1.3 | | |
| | 4 | 242 | 173 | 125 | 0.393 | 1.3 | 0.267 | 1.8 | 26 | 0.534 | 2.4 | 51 | 2.00 | 1.29 | 6 | 123 | 0.76 | *8.1* | **10.6** | 0.9 | **12.9** | **1.2** |
| AR-1-3C | 1 | 175 | 106 | 98 | 0.142 | 2.1 | 0.047 | 2.3 | 16 | 0.133 | 2.5 | 47 | 2.86 | 0.34 | 6 | 120 | 0.82 | *14.5* | **17.7** | 1.3 | | |
| | 2 | 240 | 205 | 136 | 0.482 | 1.4 | 0.133 | 1.9 | 17 | 0.494 | 2.4 | 64 | 3.71 | 0.97 | 6 | 125 | 0.80 | *15.4* | **19.4** | 1.4 | | |
| | 3 | 191 | 154 | 82 | 0.151 | 2.0 | 0.042 | 2.4 | 18 | 0.153 | 2.5 | 65 | 3.66 | 0.28 | 6 | 119 | 0.67 | *15.5* | **23.1** | 2.6 | | |
| | 4 | 180 | 121 | 75 | 0.166 | 2.0 | 0.047 | 2.3 | 22 | 0.174 | 2.4 | 80 | 3.71 | 0.27 | 6 | 124 | 0.77 | *15.1* | **19.6** | 1.7 | **19.9** | **1.1** |
| AR-2 | 1 | 180 | 127 | 77 | 0.049 | 2.9 | 0.029 | 2.9 | 14 | 0.116 | 2.5 | 56 | 4.05 | 0.36 | 6 | 176 | 0.61 | *6.9* | **11.2** | 1.5 | | |
| | 2 | 254 | 132 | 120 | 0.327 | 1.3 | 0.164 | 1.9 | 22 | 0.596 | 2.4 | 80 | 3.62 | 1.59 | 6 | 214 | 0.77 | *8.5* | **11.1** | 0.9 | | |
| | 3 | 150 | 106 | 69 | 0.048 | 3.1 | 0.024 | 3.2 | 18 | 0.106 | 2.5 | 80 | 4.45 | 0.32 | 7 | 244 | 0.56 | *7.8* | **13.9** | 2.1 | | |
| | 4 | 149 | 101 | 101 | 0.031 | 3.6 | 0.02 | 3.7 | 15 | 0.074 | 2.5 | 55 | 3.74 | 0.49 | 7 | 361 | 0.67 | *6.1* | **9.1** | 1.2 | **11.3** | **1.0** |
| AR-3 | 1 | 188 | 147 | 89 | 0.064 | 2.7 | 0.068 | 2.1 | 17 | 0.165 | 2.4 | 41 | 2.45 | 0.48 | 6 | 118 | 0.70 | *4.8* | **6.8** | 0.7 | | |
| | 2 | 258 | 206 | 90 | 0.065 | 3.0 | 0.067 | 2.0 | 16 | 0.166 | 2.4 | 39 | 2.46 | 0.48 | 5 | 114 | 0.77 | *4.8* | **6.3** | 0.6 | | |
| | 3 | 164 | 119 | 62 | 0.013 | 6.6 | 0.029 | 2.9 | 17 | 0.069 | 2.5 | 40 | 2.37 | 0.18 | 6 | 108 | 0.54 | *2.4* | **4.4** | 0.9 | | |
| | 4 | 187 | 146 | 88 | 0.048 | 2.8 | 0.048 | 2.2 | 16 | 0.119 | 2.5 | 39 | 2.45 | 0.42 | 7 | 138 | 0.66 | *5.0* | **7.5** | 0.9 | | |
| | 5 | 157 | 95 | 116 | 0.071 | 2.4 | 0.072 | 2.0 | 17 | 0.180 | 2.4 | 42 | 2.48 | 0.53 | 7 | 124 | 0.71 | *4.9* | **6.9** | 0.7 | **6.4** | **0.5** |
| AR-4 | 1 | 204 | 204 | 236 | 0.692 | 1.3 | 0.349 | 1.8 | 15 | 0.851 | 2.4 | 37 | 2.43 | 3.35 | 6 | 147 | 0.90 | *9.9* | **11.0** | 0.5 | | |
| | 2 | 189 | 164 | 108 | 0.089 | 2.6 | 0.061 | 2.1 | 14 | 0.158 | 2.5 | 37 | 2.59 | 0.60 | 6 | 138 | 0.74 | *7.2* | **9.6** | 0.9 | | |
| | 3 | 258 | 231 | 172 | 0.400 | 1.4 | 0.253 | 1.8 | 16 | 0.533 | 2.4 | 34 | 2.11 | 2.31 | 6 | 147 | 0.84 | *8.3* | **10.0** | 0.6 | | |
| | 4 | 180 | 160 | 113 | 0.092 | 2.4 | 0.078 | 2.0 | 17 | 0.221 | 2.4 | 48 | 2.84 | 0.71 | 6 | 154 | 0.75 | *5.6* | **7.5** | 0.7 | **9.5** | **0.7** |
| AR-7 | 1 | 193 | 130 | 105 | 0.086 | 2.8 | 0.058 | 2.1 | 12 | 0.209 | 2.4 | 44 | 3.61 | 0.75 | 5 | 158 | 0.70 | *6.3* | **8.9** | 1.0 | | |
| | 2 | 155 | 92 | 100 | 0.044 | 3.5 | 0.029 | 2.7 | 12 | 0.121 | 2.5 | 49 | 4.16 | 0.38 | 5 | 154 | 0.67 | *6.0* | **8.9** | 1.1 | | |
| | 3 | 181 | 136 | 114 | 0.101 | 2.4 | 0.050 | 2.1 | 11 | 0.250 | 2.4 | 54 | 5.04 | 0.75 | 5 | 160 | 0.71 | *7.2* | **10.2** | 1.1 | | |
| | 4 | 154 | 93 | 118 | 0.070 | 2.8 | 0.048 | 2.2 | 14 | 0.135 | 2.5 | 39 | 2.80 | 0.48 | 5 | 137 | 0.71 | *6.9* | **9.7** | 1.1 | **9.4** | **0.3** |
| AR-8 | 1 | 189 | 137 | 100 | 0.174 | 1.9 | 0.157 | 1.9 | 24 | 0.550 | 2.4 | 83 | 3.51 | 0.92 | 5 | 139 | 0.69 | *4.9* | **7.1** | 0.7 | | |
| | 2 | 238 | 185 | 123 | 0.097 | 2.4 | 0.082 | 1.9 | 29 | 0.236 | 2.4 | 83 | 2.90 | 0.39 | 5 | 138 | 0.75 | *5.7* | **7.6** | 0.7 | | |
| | 3 | 317 | 251 | 138 | 0.509 | 1.4 | 0.356 | 1.8 | 21 | 1.045 | 2.4 | 63 | 2.93 | 2.21 | 5 | 133 | 0.78 | *6.8* | **8.6** | 0.7 | | |
| | 4 | 128 | 94 | 66 | 0.034 | 4.2 | 0.039 | 2.3 | 22 | 0.120 | 2.5 | 67 | 3.05 | 0.23 | 5 | 129 | 0.53 | *4.0* | **7.5** | 1.2 | **7.7** | **0.3** |
| AR-12 | 1 | 170 | 113 | 88 | 0.034 | 4.3 | 0.034 | 2.7 | 17 | 0.073 | 2.5 | 37 | 2.15 | 0.22 | 9 | 111 | 0.65 | *5.3* | **8.1** | 1.1 | | |

| | | | | | | | | | | | | | | | | | | | | | |
|---|---|---|---|---|---|---|---|---|---|---|---|---|---|---|---|---|---|---|---|---|---|
| | 2 | 266 | 204 | 124 | 0.208 | 2.0 | 0.131 | 1.9 | 16 | 0.278 | 2.4 | 34 | 2.11 | 0.99 | 9 | 122 | 0.81 | *8.4* | **10.4** | 0.8 | |
| | 3 | 357 | 289 | 166 | 0.462 | 1.7 | 0.278 | 1.8 | 15 | 0.601 | 2.4 | 33 | 2.16 | 2.28 | 9 | 126 | 0.82 | *8.7* | **10.6** | 0.7 | **9.7** **0.8** |
| AR-17 | 1 | 171 | 97 | 82 | 0.029 | 4.6 | 0.029 | 2.8 | 14 | 0.071 | 2.5 | 34 | 2.43 | 0.21 | 6 | 102 | 0.63 | *5.0* | **7.9** | 1.2 | |
| | 2 | 239 | 202 | 148 | 0.227 | 1.7 | 0.136 | 1.9 | 14 | 0.253 | 2.4 | 26 | 1.86 | 1.04 | 6 | 107 | 0.81 | *9.2* | **11.3** | 0.8 | |
| | 3 | 272 | 208 | 88 | 0.076 | 2.2 | 0.070 | 2.0 | 15 | 0.176 | 2.4 | 37 | 2.52 | 0.43 | 9 | 92 | 0.68 | *5.4* | **8.0** | 0.9 | |
| | 4 | 193 | 154 | 96 | 0.096 | 2.2 | 0.07 | 2.0 | 17 | 0.144 | 2.5 | 35 | 2.05 | 0.48 | 7 | 119 | 0.68 | *7.3* | **10.8** | 1.2 | |
| | 5 | 193 | 134 | 90 | 0.062 | 2.9 | 0.066 | 2.0 | 20 | 0.150 | 2.5 | 44 | 2.27 | 0.39 | 7 | 117 | 0.66 | *4.9* | **7.5** | 0.9 | |
| | 6 | 258 | 216 | 113 | 0.138 | 1.7 | 0.099 | 1.9 | 13 | 0.251 | 2.4 | 34 | 2.54 | 0.78 | 6 | 105 | 0.74 | *6.9* | **9.4** | 0.9 | **9.1** **0.7** |
| AR-18 | 1 | 105 | 70 | 91 | 0.049 | 3.2 | 0.037 | 2.5 | 15 | 0.100 | 2.5 | 40 | 2.71 | 0.42 | 6 | 169 | 0.68 | *6.4* | **9.4** | 1.1 | |
| | 2 | 284 | 180 | 148 | 0.367 | 1.6 | 0.193 | 1.8 | 16 | 0.469 | 2.4 | 39 | 2.43 | 1.81 | 6 | 148 | 0.78 | *9.5* | **12.2** | 0.9 | |
| | 3 | 212 | 159 | 125 | 0.460 | 1.5 | 0.235 | 1.8 | 15 | 0.564 | 2.4 | 35 | 2.40 | 2.35 | 6 | 146 | 0.78 | *9.8* | **12.6** | 1.0 | **11.4** **1.0** |
| AR-19 | 1 | 197 | 135 | 100 | 0.059 | 3.2 | 0.062 | 2.1 | 14 | 0.129 | 2.5 | 30 | 2.09 | 0.56 | 6 | 129 | 0.73 | *5.1* | **7.0** | 0.7 | |
| | 2 | 167 | 121 | 82 | 0.027 | 4.4 | 0.033 | 2.7 | 15 | 0.068 | 2.5 | 31 | 2.08 | 0.28 | 6 | 126 | 0.67 | *4.4* | **6.6** | 0.9 | |
| | 3 | 189 | 152 | 90 | 0.047 | 3.5 | 0.056 | 2.1 | 16 | 0.117 | 2.5 | 34 | 2.09 | 0.41 | 6 | 118 | 0.70 | *4.5* | **6.4** | 0.8 | |
| | 4 | 169 | 121 | 97 | 0.041 | 3.8 | 0.044 | 2.3 | 16 | 0.089 | 2.5 | 32 | 2.01 | 0.32 | 6 | 115 | 0.68 | *5.1* | **7.5** | 0.9 | **6.9** **0.2** |
| AR-21 | 1 | 179 | 143 | 81 | 0.024 | 4.4 | 0.036 | 2.5 | 15 | 0.088 | 2.5 | 38 | 2.46 | 0.36 | 6 | 154 | 0.67 | *3.4* | **5.1** | 0.7 | |
| | 2 | 163 | 122 | 118 | 0.057 | 3.1 | 0.067 | 2.1 | 14 | 0.167 | 2.4 | 36 | 2.51 | 0.67 | 6 | 145 | 0.76 | *4.2* | **5.5** | 0.5 | |
| | 3 | 208 | 175 | 126 | 0.082 | 2.5 | 0.096 | 1.9 | 15 | 0.215 | 2.4 | 34 | 2.25 | 0.89 | 6 | 140 | 0.78 | *4.4* | **5.6** | 0.5 | |
| | 4 | 249 | 197 | 139 | 0.149 | 1.7 | 0.127 | 1.9 | 14 | 0.281 | 2.4 | 32 | 2.21 | 1.28 | 6 | 145 | 0.80 | *6.0* | **7.5** | 0.6 | **5.9** **0.5** |
| *Zircon (U–Th)/He ages* | | | | | | | | | | | | | | | | | | | | | |
| AR-1-1 | 1 | 222 | 112 | 88 | 8.259 | 1.0 | 2.553 | 1.8 | 491.6 | 1.242 | 2.4 | 239.1 | 0.49 | 0.020 | 12.3 | 4 | 0.772 | *23.99* | **31.10** | 2.44 | |
| | 2 | 172 | 82 | 100 | 7.313 | 1.0 | 2.383 | 1.8 | 387.3 | 0.992 | 2.4 | 161.2 | 0.42 | 0.010 | 16.1 | 2 | 0.781 | *23.11* | **29.60** | 2.25 | |
| | 3 | 220 | 105 | 99 | 8.152 | 1.0 | 2.300 | 1.8 | 348.1 | 0.970 | 2.4 | 146.8 | 0.42 | 0.018 | 13.4 | 3 | 0.790 | *26.65* | **33.73** | 2.48 | **31.5** **1.2** |
| AR-3 | 1 | 374 | 224 | 111 | 26.62 | 0.9 | 9.14 | 1.8 | 615 | 4.68 | 2.4 | 315 | 0.51 | 0.05 | 10 | 3 | 0.83 | *21.5* | **26.0** | 1.7 | |
| | 2 | 328 | 148 | 138 | 25.18 | 0.9 | 8.46 | 1.8 | 485 | 3.43 | 2.4 | 197 | 0.41 | 0.04 | 10 | 2 | 0.85 | *22.5* | **26.5** | 1.6 | |
| | 3 | 283 | 110 | 127 | 19.48 | 0.9 | 6.75 | 1.8 | 568 | 2.52 | 2.4 | 212 | 0.37 | 0.03 | 10 | 3 | 0.83 | *21.9* | **26.4** | 1.7 | |
| | 4 | 306 | 137 | 142 | 23.13 | 0.9 | 7.94 | 1.8 | 463 | 3.10 | 2.4 | 181 | 0.39 | 0.03 | 10 | 2 | 0.85 | *22.1* | **26.0** | 1.5 | **26.2** **0.1** |
| AR-4 | 1 | 345 | 171 | 156 | 30.49 | 0.8 | 9.60 | 1.8 | 392 | 4.32 | 2.4 | 176 | 0.45 | 0.09 | 10 | 4 | 0.86 | *23.7* | **27.5** | 1.5 | |
| | 2 | 351 | 159 | 150 | 26.80 | 0.8 | 9.95 | 1.8 | 451 | 4.04 | 2.4 | 183 | 0.41 | 0.20 | 10 | 9 | 0.86 | *20.3* | **23.7** | 1.3 | |
| | 3 | 524 | 306 | 145 | 39.26 | 0.8 | 12.42 | 1.8 | 355 | 5.33 | 2.4 | 152 | 0.43 | 0.36 | 10 | 10 | 0.87 | *23.7* | **27.4** | 1.5 | **26.2** **1.3** |
| AR-5 | 1 | 218 | 138 | 86 | 3.55 | 0.9 | 2.20 | 1.8 | 414 | 0.96 | 2.4 | 182 | 0.44 | 0.01 | 13 | 2 | 0.77 | *12.12* | **15.72** | 1.22 | |
| | 2 | 329 | 190 | 106 | 16.49 | 0.9 | 7.57 | 1.8 | 645 | 2.38 | 2.4 | 203 | 0.31 | 0.07 | 9 | 6 | 0.82 | *16.78* | **20.54** | 1.36 | |
| | 3 | 274 | 127 | 100 | 8.57 | 0.9 | 4.25 | 1.8 | 547 | 1.66 | 2.4 | 214 | 0.39 | 0.02 | 10 | 3 | 0.80 | *15.28* | **19.16** | 1.36 | **18.5** **1.4** |
| AR-6 | 1 | 254 | 143 | 138 | 10.16 | 1.3 | 5.14 | 1.8 | 341 | 2.04 | 2.4 | 135 | 0.40 | 0.03 | 14 | 2 | 0.84 | *15.0* | **17.7** | 1.1 | |
| | 2 | 304 | 129 | 115 | 19.65 | 1.3 | 10.04 | 1.8 | 921 | 3.94 | 2.4 | 361 | 0.39 | 0.04 | 13 | 4 | 0.82 | *14.8* | **18.1** | 1.2 | |
| | 3 | 353 | 97 | 173 | 19.86 | 1.1 | 9.65 | 1.8 | 402 | 3.83 | 2.4 | 159 | 0.40 | 0.06 | 13 | 2 | 0.87 | *15.6* | **18.0** | 1.0 | **17.9** **0.1** |
| AR-7 | 1 | 402 | 149 | 149 | 18.80 | 0.9 | 6.23 | 1.8 | 273 | 1.82 | 2.4 | 80 | 0.29 | 0.08 | 11 | 3 | 0.86 | *23.4* | **27.2** | 1.5 | |
| | 2 | 417 | 220 | 156 | 30.72 | 0.8 | 8.14 | 1.8 | 266 | 3.49 | 2.4 | 114 | 0.43 | 0.08 | 11 | 2 | 0.87 | *28.3* | **32.6** | 1.7 | |
| | 3 | 378 | 172 | 126 | 27.36 | 0.8 | 7.54 | 1.8 | 448 | 3.31 | 2.4 | 197 | 0.44 | 0.06 | 11 | 3 | 0.84 | *27.2* | **32.4** | 1.9 | **30.7** **1.8** |
| AR-8 | 1 | 347 | 152 | 148 | 28.07 | 1.4 | 12.65 | 1.8 | 492 | 5.47 | 2.4 | 213 | 0.43 | 0.12 | 6 | 5 | 0.86 | *16.7* | **19.5** | 1.2 | |
| | 2 | 340 | 155 | 150 | 19.33 | 1.4 | 8.79 | 1.8 | 391 | 4.39 | 2.4 | 195 | 0.50 | 0.09 | 5 | 4 | 0.86 | *16.3* | **19.0** | 1.1 | |
| | 3 | 340 | 165 | 148 | 18.64 | 1.4 | 8.80 | 1.8 | 390 | 3.58 | 2.4 | 159 | 0.41 | 0.09 | 6 | 4 | 0.86 | *16.0* | **18.6** | 1.1 | **19.0** **0.2** |
| AR-14 | 1 | 209 | 96 | 106 | 6.28 | 0.9 | 3.13 | 1.8 | 550 | 1.47 | 2.4 | 258 | 0.47 | 0.02 | 15 | 4 | 0.80 | *14.9* | **18.7** | 1.3 | |
| | 2 | 156 | 70 | 72 | 3.36 | 0.9 | 1.79 | 1.8 | 816 | 1.01 | 2.4 | 460 | 0.56 | 0.01 | 22 | 2 | 0.71 | *13.7* | **19.2** | 1.8 | |
| | 3 | 171 | 76 | 73 | 1.67 | 1.0 | 1.14 | 1.8 | 535 | 0.54 | 2.4 | 254 | 0.47 | 0.00 | 25 | 1 | 0.72 | *10.9* | **15.1** | 1.4 | **17.7** **1.3** |

*(continued)*

**Table 2.** (Continued)

| Sample | Aliquot | Crystal length (μm) | Prism length (μm) | Prism width (μm) | He | | $^{238}$U | | | $^{232}$Th | | | Sm | | | Ejection correction | *Uncorrected He age* | Ft-corrected He age | | Sample unweighted | |
|---|---|---|---|---|---|---|---|---|---|---|---|---|---|---|---|---|---|---|---|---|---|
| | | | | | Volume (ncc) | 1σ (%) | Mass (ng) | 1σ (%) | Concentration (ppm) | Mass (ng) | 1σ (%) | Concentration (ppm) | Th/U ratio | Mass (ng) | 1σ (%) | Concentration (ppm) | (Ft) | *(Ma)* | (Ma) | 2σ (Ma) | mean ±2 SE (Ma) | (Ma) |
| AR-15 | 1 | 133 | 68 | 70 | 2.201 | 1.1 | 1.099 | 1.8 | 502 | 0.530 | 2.4 | 242 | 0.48 | 0.01 | 13 | 6 | 0.70 | *14.9* | **21.1** | 2.0 | | |
| | 2 | 158 | 64 | 82 | 4.062 | 1.0 | 1.713 | 1.8 | 513 | 0.754 | 2.4 | 226 | 0.44 | 0.02 | 12 | 7 | 0.74 | *17.8* | **24.1** | 2.1 | | |
| | 3 | 134 | 66 | 74 | 3.108 | 1.0 | 1.402 | 1.8 | 484 | 0.390 | 2.4 | 134 | 0.28 | 0.03 | 11 | 10 | 0.72 | *17.2* | **24.1** | 2.3 | **23.1** | **1.0** |
| AR-19 | 1 | 177 | 73 | 89 | 3.66 | 0.9 | 1.86 | 1.8 | 494 | 0.76 | 2.4 | 201 | 0.41 | 0.00 | 28 | 1 | 0.76 | *14.8* | **19.5** | 1.6 | | |
| | 2 | 198 | 93 | 91 | 5.59 | 0.9 | 2.18 | 1.8 | 489 | 0.88 | 2.4 | 196 | 0.40 | 0.01 | 13 | 2 | 0.77 | *19.4* | **25.2** | 2.0 | | |
| | 3 | 207 | 100 | 81 | 6.96 | 0.9 | 2.22 | 1.8 | 763 | 1.04 | 2.4 | 358 | 0.47 | 0.00 | 23 | 1 | 0.75 | *23.3* | **31.0** | 2.6 | | |
| | 4 | 224 | 116 | 100 | 7.50 | 0.9 | 3.63 | 1.8 | 541 | 1.44 | 2.4 | 215 | 0.40 | 0.04 | 10 | 6 | 0.79 | *15.6* | **19.7** | 1.4 | **23.8** | **2.7** |
| AR-21 | 1 | 296 | 97 | 134 | 14.05 | 0.8 | 6.30 | 1.8 | 519 | 2.47 | 2.4 | 204 | 0.39 | 0.03 | 10 | 2 | 0.835 | *16.9* | **20.2** | 1.2 | | |
| | 2 | 328 | 127 | 144 | 14.92 | 0.8 | 8.37 | 1.8 | 509 | 3.77 | 2.4 | 229 | 0.45 | 0.03 | 9 | 2 | 0.849 | *13.3* | **15.7** | 0.9 | | |
| | 3 | 296 | 124 | 136 | 13.47 | 0.9 | 6.27 | 1.8 | 479 | 2.60 | 2.4 | 198 | 0.41 | 0.02 | 13 | 1 | 0.842 | *16.2* | **19.2** | 1.2 | **18.4** | 1.4 |

The volume of He is given in nanocubic centimetres at standard temperature and pressure. The ejection correction (Ft) is the correction factor for alpha-ejection (according to Farley *et al.* 1996). The uncertainties in the contents of He and radioactive elements are given as 1σ values in relative error (%). The uncertainty of the single grain ages is given as 1σ values and includes both the analytical uncertainty and the estimated uncertainty of Ft. The uncertainty of the mean sample ages are one standard error as $(SD)/(n)^{1/2}$, where SD is the standard deviation of the age replicates and $n$ is the number of age determinations. Uncorrected and corrected ages are highlighted by italic and bold type, respectively.

preliminary modelling runs indicating that their variation within plausible limits did not significantly influence the modelling results. The values that were fixed in the model include the age of the Oligocene and Miocene volcanism, the thickness of the Oligo-Miocene sedimentary cover, the heat flux until Miocene volcanism, the petrophysical values (e.g. thermal conductivity, heat capacity, heat production) and the compaction characteristics of the sediments.

The modelling was performed separately on each previously defined age group (Fig. 5). These age groups are considered to represent rock volumes within the Recsk Complex that experienced uniform thermal histories. The mean depths of these groups were considered in the one-dimensional subsidence modelling procedure. It was not possible to modify all the parameters in a simple one-dimensional subsidence model, therefore two parameters were tested in one batch and the rest of the input data was kept fixed. The flow chart in Figure 7 summarizes the major steps of the tandem modelling. The modelling of an age group was performed in different batches, where different parameters were selected as variables while others were kept constant. In this way, we were able to create a multi-parameter probability space marking the most likely conditions that resulted in the measured He ages.

### *First step: modelling of burial temperature*

The PetroMod 1D software (Schlumberger) was used for modelling the subsidence/thermal history of the Recsk Complex. In the input part, we set the fixed parameters and possible ranges of the variables according to regional geological constraints and analogies (Table 4). A 1000 m thick diorite–andesite layer was set for the lowest member of the one-dimensional rock column (representing the Recsk Complex). This is a reliable assumption as such a lithology was revealed by >100 boreholes and several adits. Its cover was determined according to the Rm-103 borehole, which intersected the complete Oligo-Miocene sedimentary and volcano-sedimentary sequence covering the Recsk Complex. According to this borehole and the surface outcrops of these formations, an average thickness of 500 m was considered for the Oligo-Miocene clastic sequence. It is assumed that these sediments were also covered by the Miocene Mátra Volcano, although its former thickness is not known. Therefore the thickness of the Mátra volcanic rocks (variable 3, Fig. 6) was varied between 0 and 2500 m. The heat flux was set to a typical continental value of 60 mW m$^{-2}$ (Pollack *et al.* 1993 and references cited therein) between 30 and 20 Ma, followed by a linear increase until 18 Ma to today's local value (100 mW m$^{-2}$) because of the assumed start of the synrift phase of the Pannonian Basin between 20 and 18 Ma (Royden & Horváth 1988). The increased heat flux due to Mátra volcanism is described by two variables, namely the value of the increased heat flux and the duration of this effect (variables 1 and 2, Fig. 6). The heat flux was varied between 110 and 300 mW m$^{-2}$ and the duration was varied between 0.5 and 1.5 Ma. The trend of the increase and decrease in heat flux was assumed to be linear. According to sensitivity tests, the style (curvature) of the increase and decrease have negligible effect on the thermal history and calculated He ages. The termination of the increased heat flux plateau was fixed at 14 Ma, so that the maximum heat flux coincided with the main activity of the Mátra Volcano (16–14 Ma, Zelenka *et al.* 2004).

After the main activity of the Mátra Volcano, erosion took place in the area, which affected the Mátra volcanic rocks, the Oligo-Miocene sediments and the Recsk Complex. However, the erosion did not cut deep into the Recsk Complex because remnants of the overlying Late Oligocene glauconitic sandstone have been preserved in some places (Fig. 2). Therefore, for

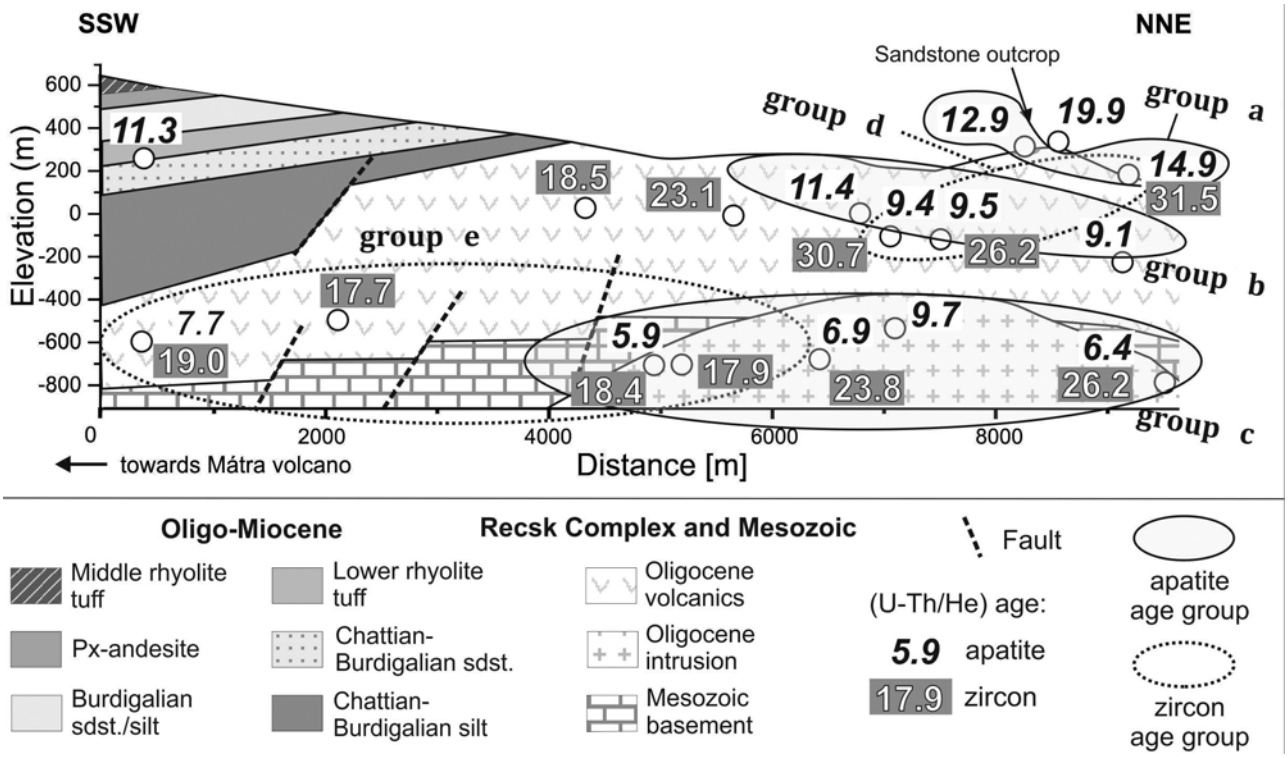


**Fig. 5.** Simplified SSW–NNE cross-section (identical to the section in Fig. 2b) across the Recsk Complex with the AHe and ZHe ages and their groupings. The positions of the samples were projected orthogonally to the section (for sample codes, see Fig. 2). Each presented He age is the unweighted average of three to six single-crystal ages corrected for ejection factors; for details and uncertainties, see Table 1. px, pyroxene.

modelling the subsidence–exhumation history, complete removal of the Oligo-Miocene cover sequences was assumed in all runs, whereas no erosion of the Recsk Complex was considered. The Miocene erosion rate was also considered in the model because it had a significant influence on the thermal history. To account for changes in the erosion rate, two further variables were introduced: the time when the erosion rate changed (variable 4) and the depth of the current surface at that time (i.e. the thickness of the remaining cover, variable 5, Fig. 6). The age of the change in the erosion rate was varied between 12 and 4 Ma and its depth was varied between 900 and 0 m (0 m means complete exhumation at that time). Thus variable erosion scenarios could be modelled, such as steady, initially slow – then fast, initially fast – then slow. The thermal history was calculated in this way for each erosion scenario.

### *Second step: modelling the ZHe and AHe ages*

The thermal evolution paths (Fig. 7) obtained in the first modelling step were imported into the HeFTy software (Ketcham 2005) to calculate AHe and ZHe ages. The properties of the dated crystals of each group – such as average sphere radius and U, Th and Sm concentrations – were also taken into consideration.

**Table 3.** *Modelling groups, used for modelling the thermal history of the Recsk Complex using the PetroMod 1D software.*

| Modelling group | Depth (m) | Mean ± SD He age (Ma) |
|---|---|---|
| a | 0 | AHe 14.2 ± 2.1 |
| b | 350 | AHe 9.7 ± 1.5 |
| c | 910 | AHe 6.4 ± 1.0 |
| d | 240 | ZHe 29.5 ± 3.3 |
| e | 1030 | ZHe18.3 ± 1.5 |

### *Outlining the acceptance belt of the tested parameter pairs*

The tandem modelling was performed in batches, where the two tested parameters were modified stepwise, ultimately yielding an age matrix (Fig. 7). These matrices contained the calculated He ages and, using contouring methods (kriging), the belt of acceptance could be visualized. The belt of acceptance represents the area in which the calculated ages match the measured (U–Th)/He age data. By comparing the results and acceptance belts of different batches, it was possible to mark the most reliable values of the tested parameters for some of the measured age groups. In doing so, the burial/thermal evolution of the Recsk Complex could be much better constrained.

**Table 4.** *Fixed values and variable parameters applied for modelling the thermal history of the Recsk Complex using the PetroMod 1D software.*

| | | |
|---|---|---|
| Fixed values used for modelling | | |
| | Thickness of Oligo-Miocene sedimentary sequence | 500 m |
| | Heat flux between 30 and 20 Ma | 60 mW $m^{-2}$ |
| | Heat flux between 20 and 18 Ma | Linear increase to 100 mW $m^{-2}$ |
| | Heat flux after 18 Ma (in the non-volcanic period) | Linear decrease from 110 to 100 mW $m^{-2}$ |
| | Duration of period of increasing and decreasing heat flux before and after the volcanism | 0.25 myr |
| Variable parameters | | |
| 1 | Miocene heat flow increased by volcanism | 110–300 mW $m^{-2}$ |
| 2 | Duration of the increased heat flow | 0.5–1.5 myr |
| 3 | Thickness of the Miocene volcanic cover | 0–2500 m |
| 4 | Time at which the erosion rate changed | 12–4 Ma |
| 5 | Thickness of the remaining cover when the erosion rate changed | 0–900 m |

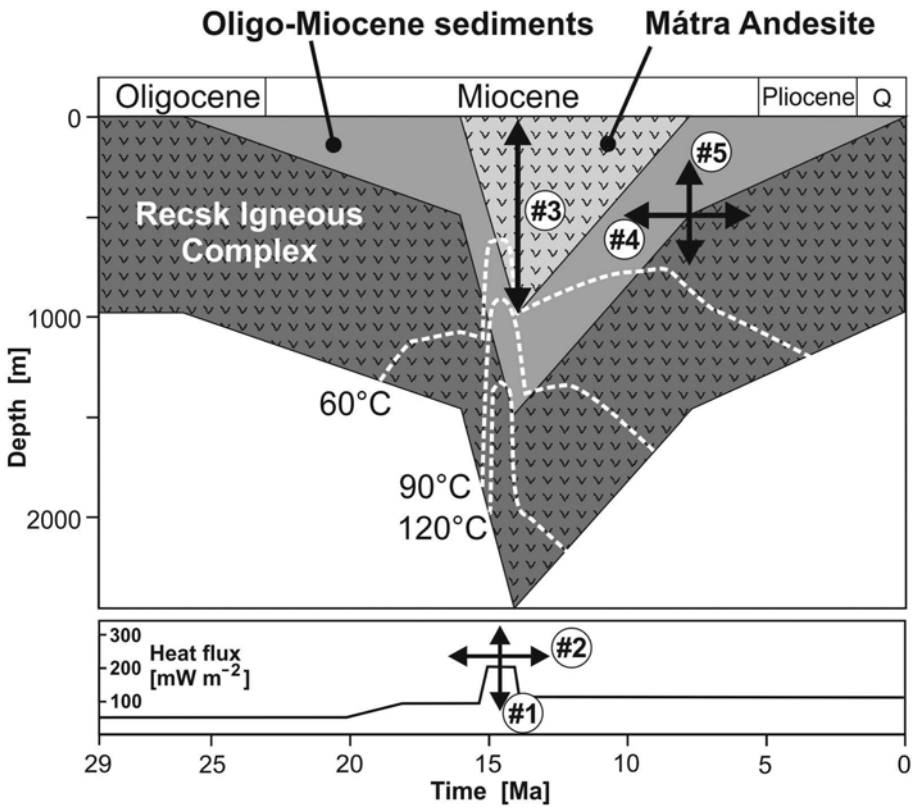


**Fig. 6.** Schematic diagram of the assumed burial history of the Recsk Complex. The arrows represent the variable parameters: 1, the value of the increased Miocene heat flux during Mátra volcanism; 2, the duration of the increased heat flux; 3, the thickness of the Miocene volcanic cover; 4, the time when the erosion rate had changed; and 5, the thickness of the remaining cover at the time when the erosion rate had changed. Isotherms (dashed lines) are given as examples only and represent one given modelling run. Their position is controlled by the values of the variable parameters and some fixed parameters (e.g. the thickness of Oligo-Miocene sediments).

## Discussion

After some preliminary modelling runs, it became obvious that the He ages were virtually independent from some of the variables in given age groups, thus it was possible to reduce the number of variable pairs tested.

First, the sensitivity of the ZHe ages on each variable was tested. The different heat flux values obtained by changing the value of the Miocene heat flux (parameter 1) modified the thermal history in and above the zircon PRZ, resulting in significantly different ZHe ages. By contrast, the duration of the increased heat flux (parameter 2) was shown to have only a minor effect on the ZHe ages (Fig. 8a). Further modelling runs showed that the thickness of the Miocene volcanic cover (parameter 3) exerted a strong control over the ZHe ages (Fig. 8b). Importantly, the value of the Miocene heat flux and the Miocene volcanic cover (parameters 1 and 3, respectively) interacted multiplicatively, meaning that the same ZHe age may have resulted from either a higher heat flux and a thinner cover or a thicker cover and a lower heat flux. The time and depth of the erosion breakpoint (parameters 4 and 5) was chosen for the batch calculations according to the assumptions of the preliminary runs that yielded reasonable AHe and ZHe ages. Their value had a negligible effect on the ZHe ages because the depth of the breakpoint was limited by the thickness of the volcanic cover (0–2500 m), so the temperature at this point was always below the zircon PRZ. Therefore the only parameters that significantly affected the ZHe ages were the duration of the increased Miocene heat flux and the cover thickness. Therefore only these two parameters were treated as variables in the ZHe modelling runs, whereas the other three parameters were kept constant. For simplicity, the post-climax trend of the erosion was fixed in the form of steady erosion and the duration of the increased heat flux was fixed at 1 myr, which is a geologically realistic assumption due to the relatively short activity of the Mátra Volcano (Zelenka *et al.* 2004).

Unlike the ZHe ages, the AHe ages show no dependence on the value and duration of the Miocene volcanic activity or on the cover thickness (parameters 1, 2 and 3, respectively). This can be explained by the fact that the vast majority of the AHe ages is younger than the Mátra volcanism, meaning that the ages are totally reset (except group a) and the details of the thermal climax are irrelevant. Because the AHe method has an extremely low closure temperature of *c.* 60°C, even half a million years at a heat flux of 150 mW m$^{-2}$ with shallow burial could cause a complete reset of the AHe ages and a longer and/or stronger heat pulse could not modify this any further. By contrast, the AHe ages proved to be extremely sensitive to the time and depth of the erosion breakpoint (parameters 4 and 5) because a change in these two parameters modified the thermal history in the apatite PRZ (Fig. 6). Based on these observations, the value of the Miocene heat effect could be fixed at 200 mW m$^{-2}$, its duration at 1 Ma and the Miocene volcanic cover thickness at 1000 m in the AHe modelling runs.

### *Thermal history reconstruction based on ZHe ages*

The oldest and unreset ZHe ages were detected in group d, occupying a shallow position within the Recsk Complex (Fig. 5). The average ZHe age of *c.* 29.5 Ma is identical to the emplacement age of the complex and therefore this part of the Recsk Complex was not in the zircon PRZ (for a considerable amount of time) in post-Oligocene times. Because the ZHe ages of the group roughly equal the formation age, the modelling did not yield a narrow belt, but a broad range of acceptable values, illustrating the possible maximum values and their dependence on the main controlling parameters, i.e. the thickness of volcanic cover and the heat flux (Fig. 9).

In turn, the partially reset ZHe ages of group e are significantly younger than the emplacement age of the Recsk Complex, reflecting a thermal overprint that exceeded the closure temperature of the ZHe thermochronometer. These samples became thermally reset because group e is situated deeper and closer to the Mátra heat source than group d (Fig. 5). The modelling results of group e yield a probability belt for the possible interdependence of volcanic burial and heat flux (Fig. 8b) that can be overlapped with the possible maximum values calculated using the non-reset group d (Fig. 9). This overlap, reflecting consistent modelling results for rather contrasting groups

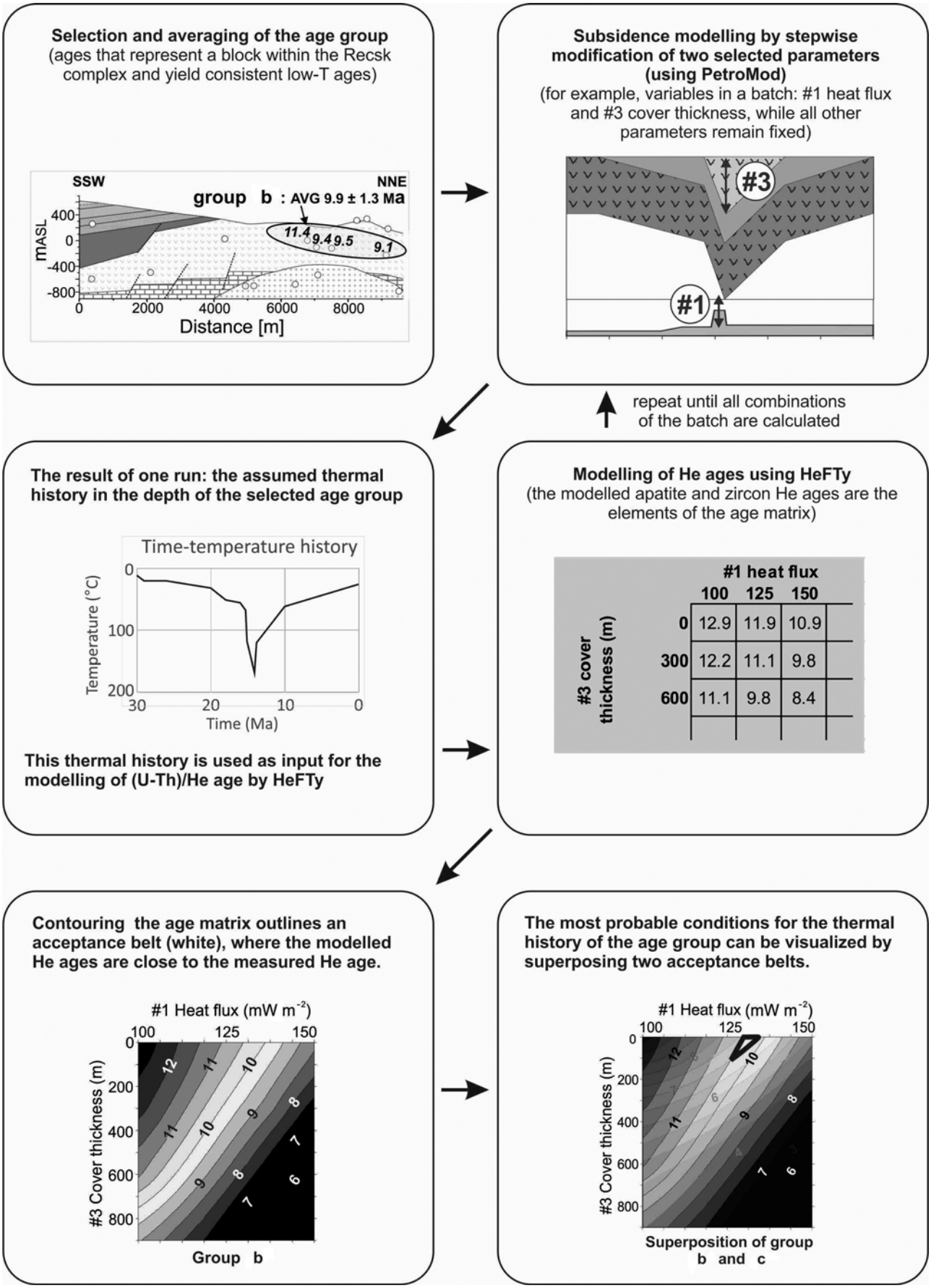


**Fig. 7.** Flow chart of the modelling procedure. The Schlumberger PetroMod one-dimensional software was used for modelling the thermal history during burial and HeFTy software (Ketcham 2005) was used to calculate the (U–Th)/He ages. The thick black triangle on the lower right-hand diagram marks the most probable conditions of the thermal evolution obtained by modelling.

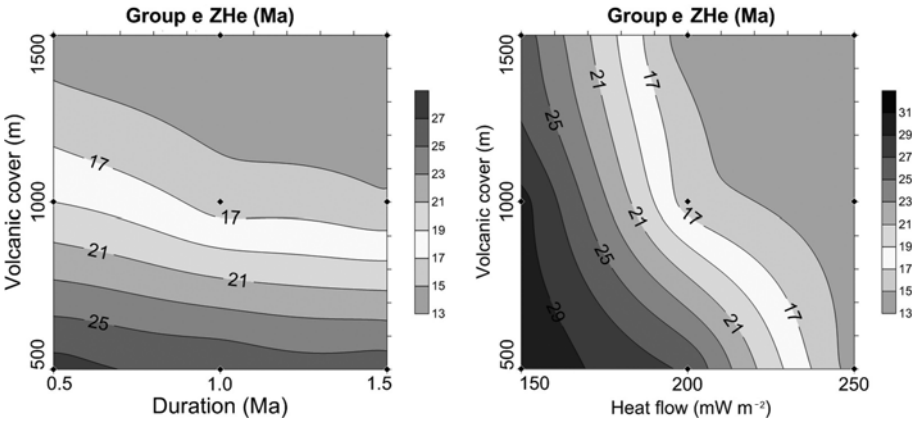


**Fig. 8.** Thermal modelling results of the ZHe age group e in the Recsk Complex (the southern, deeper part of the complex with 18.3 ± 1.5 Ma ZHe group age; see Fig. 5). Plots show the dependence of the calculated ZHe ages (isolines) on the cover thickness and the (**a**) duration and (**b**) heat flux of the Miocene magmatism. The fixed parameters include (**a**) the 200 mW $m^{-2}$ Miocene heat flux and steady erosion or (**b**) the 1 myr duration of Miocene volcanism and steady erosion. The belts of best fit are marked in white; the gradation of shading implies an increasingly poorer fit.

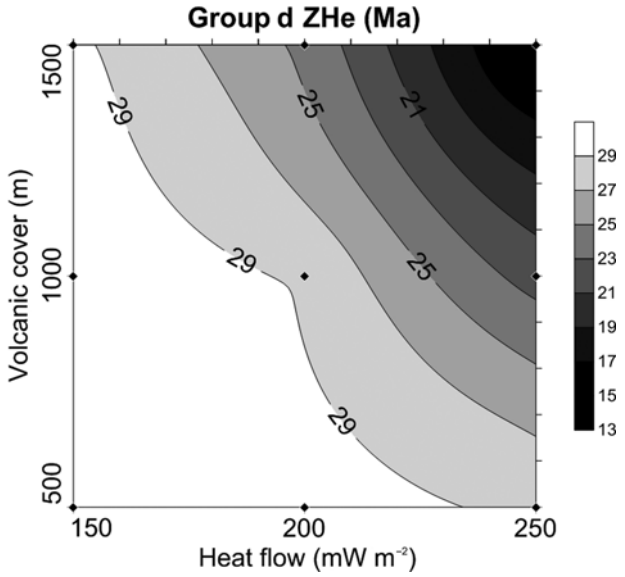


**Fig. 9.** Modelled ZHe ages (isolines) of age group d (the northern, shallow part of the complex with 29.5 ± 3.3 Ma ZHe group age; see Fig. 5). Fixed parameters: 1 myr duration of the Miocene magmatism (parameter 2); and steady erosion (parameters 4 and 5). As these samples yield no detectable reset from their initial *c.* 30 Ma age of formation, the acceptable burial and heat flux conditions occupy the lower left-hand half of the parameter field (in white).

of measured ages, is at roughly 200 mW $m^{-2}$ heat flux and 1000 m volcanic (and 1500 m total) cover. These values give a rough estimate of both parameters, although, due to the lateral distance between groups d and e and the probable north–south gradient in both parameters, it is unclear in which part of the complex they are valid.

### *Final stage of the thermal history based on AHe ages*

The vertical trend in the AHe ages across the Recsk Complex is obvious, as illustrated by age groups a, b and c in Figure 5. The uppermost group shows AHe ages close to the formation age of the Mátra volcanism, whereas the lower groups experienced thermal reset in the Late Miocene, which clearly post-dates the activity of Mátra Volcano. First, we modelled groups b and c because they represent completely reset AHe ages controlled exclusively by the post-volcanic exhumation history of the Recsk Complex. These two groups are located above each other, at *c.* 600 m vertical distance, and experienced the same cooling history. Therefore only those modelling results where the calculated AHe ages matched the measured ages of both age groups were accepted (group b, 9.9 ± 1.0 Ma; group c, 7.2 ± 1.7 Ma).

Figure 10 shows the results of the two age groups and their acceptance belts. The overlapping of the two acceptance belts yielded a small range for the breakpoint in exhumation between 0 and maximum 150 m volcano-sedimentary cover and 6.5–7.5 Ma, with the best fit at *c.* 7 Ma and 0 m. Thus the Mátra Volcano experienced fast erosion after the termination of volcanism until *c.* 7 Ma and the currently exhumed top of the Oligocene magmatic rocks had already reached the surface (or occupied a very shallow position) by the end of the Miocene. This result is supported by the relatively low relief of the Recsk region, suggesting a moderate present day erosion rate.

It is important to emphasize that the completely reset AHe ages (groups b and c) do not carry information on the value of the Miocene heat flux and the cover thickness. By contrast, group a yielded AHe

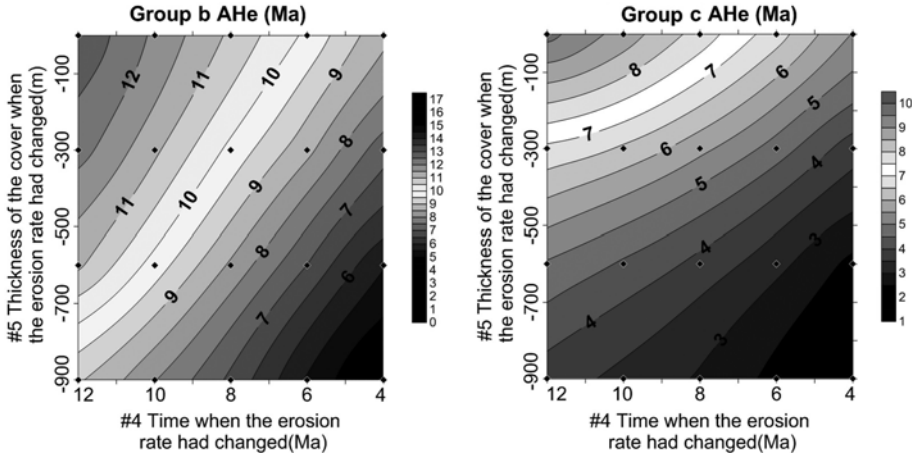


**Fig. 10.** Results of the final exhumation modelling of the Recsk Igneous Complex using two AHe age groups (groups b and c) of samples that experienced the post-volcanic (Mátra) cooling at different depths. The AHe group ages are 9.7 ± 1.5 and 6.4 ± 1.0 Ma, respectively. Fixed parameters: 1 Ma duration and 200 mW $m^{-2}$ heat flux during the Miocene volcanism and 1500 m cover thickness. The best-fitting belts of the two groups overlap at the *c.* 7 Ma change in erosion rate and negligible volcano-sedimentary cover at that time (almost complete exposure).

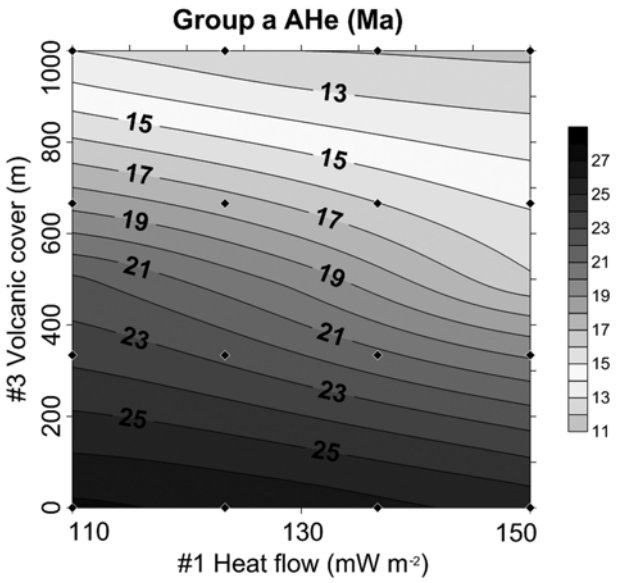


**Fig. 11.** Modelling results of AHe group a (mean AHe age 14.2 ± 2.1 Ma). Fixed parameters: age and depth of the erosion breakpoint of 6.5 Ma and 0 m. According to the acceptance belts generated, the main control parameter was the cover thickness, whereas the duration of the Miocene volcanism had less influence on the AHe ages.

ages close to the age of the Mátra volcanism (i.e. partially reset AHe ages) and therefore modelling based on these ages may constrain both the cover thickness and heat flux. We could keep the post-Mátra cooling trend fixed for these modelling runs based on the modelling results for groups b and c. We assumed that a Miocene heat flux value >150 mW $m^{-2}$ was not realistic at this distance from the Mátra Volcano. Likewise, the present day lower heat flux at Recsk (100–110 mW $m^{-2}$) seemed unrealistic. It could be also assumed that the thickness of the volcanic cover decreased with increasing distance from the Mátra volcanic centre. Consequently, the modelling parameters and their variability for group a were set in accordance with the previous assumptions. From these runs, it turned out that the AHe ages of group a were mainly determined by the cover thickness, whereas the duration and magnitude of the Miocene heat flux had only a minor influence, at least over this limited heat flux range (Fig. 11). Thus the overall cover thickness in the northern part of the study area could be estimated, with the most probable values between 1200 and 1500 m (700–1000 m volcanic cover, respectively; Fig. 11), bearing in mind that this part of the modelling is based on several assumptions, most importantly a narrow heat flux range relative to the other modelling runs.

The modelling results are in accordance with regional geological observations. The significant post-Oligocene burial and heating are also evidenced by abundant hydrocarbon films and cavity fillings in the high-porosity upper part of the Recsk Complex (Kitaibel 1829; Molnár *et al.* 2008; Takács *et al.* 2017), obviously post-dating the Oligocene emplacement and ore formation. The increased heat flux in the Miocene most probably led to maturation of the formations rich organic material in the surroundings of the Recsk Complex and triggered hydrocarbon migration. However, apart from some late calcite veins, there is no evidence for large-scale Miocene hydrothermal circulation and related ore mineralization at the Recsk Complex.

The fact that both an increased Miocene heat flux and the thermal blanketing effect of the cover strata were needed to reset the AHe and especially the ZHe ages is evident from the regional geological constraints and from studies in which the thermal effects of intrusions were modelled (e.g. Ehlers 2005). Considering no increased heat flux relative to today's value in the study area (100–110 mW $m^{-2}$), even a 3000 m thick cover would be insufficient to partially reset the ZHe ages. However, an intrusion 5 km in diameter would only locally increase the temperature up to the ZHe PRZ (<10 km from the intrusion centre; Ehlers 2005). As there is no evidence for any of these extremities (i.e. an extremely thick cover or large Miocene subvolcanic body), the combined thermal effect of magmatism and burial is plausible.

The erosion of the post-Oligocene cover sequences is underlined by the southwards tilted layers in the southern foreland of the Mátra Volcano as well as its sharp erosional termination in the north. The tilting and subsequent erosion is probably related to the opening (presumably between 14.5 and 13.5 Ma; Tari *et al.* 1993; Petrik *et al.* 2014) of the Vatta-Maklár Trough, a large-scale extensional structure *c.* 40 km to the SE of the study area.

## Conclusions

The fact that the Miocene (*c.* 15 Ma) volcano of Mátra developed on an older, currently well exposed igneous complex offers an excellent site for studying and testing the thermal influence of a stratovolcanic edifice on its basement. The well-constrained and rather uniform Early Oligocene (*c.* 30 Ma) emplacement age of the Recsk Complex allows us to calculate the degree of reset of (U–Th)/He ages primarily caused by Miocene volcanism.

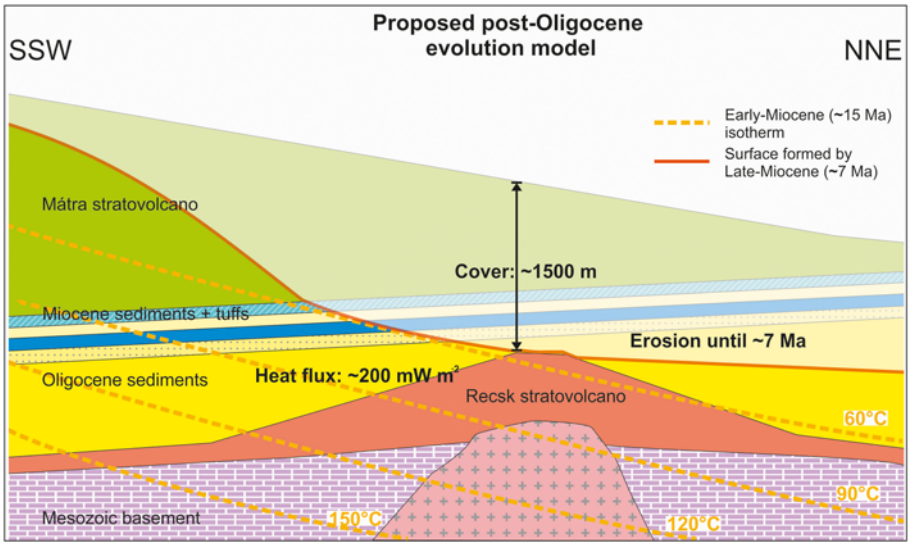


**Fig. 12.** Schematic diagram of the post-Oligocene thermal evolution of the Recsk Complex. The bold values summarize the results obtained by ZHe and AHe modelling. The semi-transparent area indicates the eroded units. See Figure 2 for legend.

Most of the ZHe ages are younger than the formation age of the Recsk Complex. Only samples from shallow levels and from larger distances from the Miocene Mátra Volcano show ages that have not been reset, whereas in the SW of the complex the younger, partially reset ZHe ages indicate an increasing thermal effect towards the Mátra volcanic centre. By contrast, the AHe ages are completely reset, except for a few samples at the surface. This implies a long-lasting cooling resulting from the thermal blanketing effect caused by the burial of the subsequently eroded stratovolcanic succession that covered the Recsk Complex in the Middle Miocene.

To quantify the parameters of the thermal and burial history, one-dimensional tandem modelling was carried out on the Recsk Complex. The ZHe modelling results let us to conclude that *c.* 1500 m thick sedimentary and volcanic cover, in addition to an elevated Miocene heat flux, was needed to partially reset the ZHe ages, both of which can be related to the Mátra Volcano (Fig. 12). AHe modelling helped us to reconstruct the erosion history of the Oligocene basement and showed that the Miocene volcanic activity was followed by rapid erosion, leading to the complete exhumation of the Recsk Complex, until the latest Miocene (*c.* 7 Ma).

**Acknowledgements** Róbert Arató visited Göttingen, studied the analytical methods and realized the helium thermochronology part of the study with the help of the Erasmus Fellowship Programme. We gratefully acknowledge the donation of samples by the Mining Museum of Recsk. We are indebted to Irina Ottenbacher and Judit Dunklné-Nagy for the careful mineral separation and for the He measurements, and to the Central Metal Workshop of the Geoscience Centre Göttingen for the maintenance of the GÖochron Laboratory. Róbert Arató thanks Tamás Garamhegyi for drawing the relief map of the Recsk Complex. We are grateful to Tibor Zelenka for providing us with his hand drawing of the Mátra stratigraphic column as well as to Kata Molnár, László Fodor, Réka Lukács, László Lenkey and Csaba Szabó, who provided useful remarks and detailed information about the regional geology. Tamás Mikes and József Pálfy are thanked for their instructive criticism. The thoughtful and detailed reviews of Konstanze Stübner and Ruohong Jiao are gratefully acknowledged as they greatly improved the quality of the manuscript. Róbert Arató also thanks Miklós Arató, Gabriella Obbágy and József Kovács for their great help and encouragement before and during the preparation of the manuscript.

**Funding** This research received no specific grant from any funding agency in the public, commercial, or not-for-profit sectors.

*Scientific editing by Yuntao Tian*

## References

Baksa, C., Csillag, J., Földessy, J. & Zelenka, T., 1981. A hypothesis about the tertiary volcanic activities of the Mátra Mountains, NE Hungary. *Acta Geologica Hungarica*, **24**, 337–349.

Benedek, K. 2002. Paleogene igneous activity along the easternmost segment of the Periadriatic-Balaton Lineament. *Acta Geologica Hungarica*, **45**, 359–371.

Bergomi, M.A., Zanchetta, S. & Tunesi, A. 2015. The Tertiary dike magmatism in the Southern Alps: geochronological data and geodynamic significance. *International Journal of Earth Sciences*, **104**, 449–473.

Dodson, M.H. 1973. Closure temperature in cooling geochronological and petrological systems. *Contributions to Mineralogy and Petrology*, **40**, 259–274.

Ehlers, T.A. 2005. Crustal thermal processes and the interpretation of thermochronometer data. *Reviews in Mineralogy and Geochemistry*, **58**, 315–350.

Exner, C. 1976. Die geologische Position der Magmatite des periadriatischen Lineamentes. *Verhandlungen der Geologischen Bundesanstalt*, **2**, 3–64.

Farley, K.A. 2002. (U–Th)/He dating: techniques, calibrations, and applications. *Reviews in Mineralogy and Geochemistry*, **47**, 819–844.

Farley, K., Wolf, R. & Silver, L. 1996. The effects of long alpha-stopping distances on (U–Th)/He ages. *Geochimica et Cosmochimica Acta*, **60**, 4223–4229.

Flowers, R.M., Shuster, D.L., Wernicke, B.P. & Farley, K.A. 2007. Radiation damage control on apatite (U–Th)/He dates from the Grand Canyon region, Colorado Plateau. *Geology*, **35**, 447–450.

Flowers, R.M., Ketcham, R.A., Shuster, D.L. & Farley, K.A. 2009. Apatite (U–Th)/He thermochronometry using a radiation damage accumulation and annealing model. *Geochimica et Cosmochimica Acta*, **73**, 2347–2365.

Földessy, J. & Szebényi, G. 2008. The mineralizations of the Recsk Deeps and Lahóca—short geological overview. *In:* Földessy, J. & Hartai, É. (eds) *Recsk and Lahóca. Geology of the Paleogene ore complex.* University of Miskolc, Series A, Mining, **73**, 85–98.

Földessy, J., Zelenka, T., Benedek, K., Pécskay, Z. & Mádai, F. 2008. The Recsk Paleogene magmatism in a regional context. *In:* Földessy, J. & Hartai, É. (eds) *Recsk and Lahóca. Geology of the Paleogene ore complex.* University of Miskolc, Series A, Mining, **73**, 129–143.

Frei, D. & Gerdes, A. 2009. Precise and accurate in situ U–Pb dating of zircon with high sample throughput by automated LA-SF-ICP-MS. *Chemical Geology*, **261**, 261–270.

Gehrels, G.E., Valencia, V.A. & Ruiz, J. 2008. Enhanced precision, accuracy, efficiency, and spatial resolution of U-Pb ages by laser ablation–multi-collector–inductively coupled plasma–mass spectrometry. *Geochemistry, Geophysics, Geosystems*, **9**, https://doi.org/10.1029/2007GC001805

Guenthner, W.R., Reiners, P.W., Ketcham, R.A., Nasdala, L. & Giester, G. 2013. Helium diffusion in natural zircon: radiation damage, anisotropy, and the interpretation of zircon (U–Th)/He thermochronology. *American Journal of Science*, **313**, 145–198.

Gyalog, L. 2013. *Geological map of Hungary, 1:500 000*. Geological and Geophysical Institute of Hungary, Budapest.

Harangi, S., Downes, H. & Seghedi, I. 2006. Tertiary-Quaternary subduction processes and related magmatism in the Alpine-Mediterranean region. *In*: Gee, D.G. & Stephenson, R.A. (eds) *European Lithosphere Dynamics. Geological Society, London, Memoirs*, **32**, 167–190, https://doi.org/10.1144/GSL.MEM.2006.032.01.10

Herman, F., Braun, J., Senden, T.J. & Dunlap, W.J. 2007. (U–Th)/He thermochronometry: mapping 3D geometry using micro-X-ray tomography and solving the associated production–diffusion equation. *Chemical Geology*, **242**, 126–136.

Jackson, S.E., Pearson, N.J., Griffin, W.L. & Belousova, E.A. 2004. The application of laser ablation-inductively coupled plasma-mass spectrometry to in situ U–Pb zircon geochronology. *Chemical Geology*, **211**, 47–69.

Ketcham, R.A. 2005. Forward and inverse modeling of low-temperature thermochronometry data. *Reviews in Mineralogy and Geochemistry*, **58**, 275–314.

Kitaibel, P. 1829. *Hydrographia Hungariae I–II*. Schuster, J. (ed.), Trattner, Pest, 162–204.

Košler, J. & Sylvester, P.J. 2003. Present trends and the future of zircon in geochronology: laser ablation ICPMS. *Reviews in Mineralogy and Geochemistry*, **53**, 243–275.

Kovács, I. & Szabó, C. 2008. Middle Miocene volcanism in the vicinity of the Middle Hungarian zone: evidence for an inherited enriched mantle source. *Journal of Geodynamics*, **45**, 1–17.

Kovács, I., Csontos, L., Szabó, C., Bali, E., Falus, G., Benedek, K. & Zajacz, Z. 2007. Paleogene–early Miocene igneous rocks and geodynamics of the Alpine-Carpathian-Pannonian-Dinaric region: an integrated approach. *In*: Beccaluva, L., Bianchini, G. & Wilson, M. (eds) *Cenozoic Volcanism in the Mediterranean Area*. *Geological Society of America, Special Papers*, **418**, 93–112.

Kupi, L. 2006. *Hydrothermal alterations at the northern part of the Lahóca Hill, NE-Hungary.* Diploma thesis, Eötvös University *[in Hungarian with English abstract]*.

Less, G., Báldi-Beke, M., Pálfalvi, S., Földessy, J. & Kertész, B. 2008. New data on the age of the Recsk volcanics and of the adjacent sedimentary rocks. *Publications of the University of Miskolc, A*, **73**, 57–84.

Ludwig, K. 2012. *User's Manual for Isoplot 3.75: a Geochronological Toolkit for Microsoft Excel*. Berkeley Geochronology Center, Special Publications, **5**.

Lukács, R., Harangi, S.*et al.*, 2018. Early to Mid-Miocene syn-extensional massive silicic volcanism in the Pannonian Basin (East-Central Europe): eruption chronology, correlation potential and geodynamic implications. *Earth-Science Reviews*, **179**, 1–19.

McDougall, I. & Harrison, T.M. 1999. *Geochronology and Thermochronology by the $^{40}Ar/^{39}Ar$ Method*. Oxford University Press, New York.

Meesters, A. & Dunai, T. 2002*a*. Solving the production–diffusion equation for finite diffusion domains of various shapes: Part I. *Implications for low-temperature (U–Th)/He thermochronology. Chemical Geology*, **186**, 333–344.

Meesters, A. & Dunai, T. 2002*b*. Solving the production–diffusion equation for finite diffusion domains of various shapes: Part II. Application to cases with α-ejection and nonhomogeneous distribution of the source. *Chemical Geology*, **186**, 347–363.

Molnár, F., Jung, P., *et al*. 2008. Epithermal zones of the porphyry-skarn-epithermal ore complex at Recsk. *In*: Földessy, J.v & Hartai, É. (eds) *Recsk and Lahóca. Geology of the Paleogene ore complex*. University of Miskolc, Series A, Mining, **73**, 99–128.

Pamič, J., Balen, D. & Herak, M. 2002. Origin and geodynamic evolution of Late Paleogene magmatic associations along the Periadriatic-Sava-Vardar magmatic belt. *Geodinamica Acta*, **15**, 209–231.

Pécskay, Z., Edelstein, O., Seghedi, I., Szakacs, A., Kovacs, M., Crihan, M. & Bernad, A. 1995*a*. K-Ar datings of Neogene-Quaternary calc-alkaline volcanic rocks in Romania. *Acta Vulcanologica*, **7**, 53–62.

Pécskay, Z., Lexa, J. *et al.* 1995*b*. Space and time distribution of Neogene-Quaternary volcanism in the Carpatho-Pannonian region. *Acta Vulcanologica*, **7**, 15–28.

Petrik, A., Beke, B. & Fodor, L. 2014. Combined analysis of faults and deformation bands reveals the Cenozoic structural evolution of the southern Bükk foreland (Hungary). *Tectonophysics*, **633**, 43–62.

Póka, T. 1988. Neogene and Quaternary volcanism of the Carpathian-Pannonian region: changes in chemical composition and its relationship to basin formation. *In*: Royden, L.H. & Horváth, F. (eds) *The Pannonian Basin: a Study in Basin Evolution*. *American Association of Petroleum Geologists, Memoir*s, **45**, 257–277.

Pollack, H.N., Hurter, S.J. & Johnson, J.R. 1993. Heat flow from the Earth's interior: analysis of the global data set. *Reviews of Geophysics*, **31**, 267–280.

Reid, M.R. 2008. How long does it take to supersize an eruption? *Elements*, **4**, 23–28.

Reiners, P.W., Spell, T.L., Nicolescu, S. & Zanetti, K.A. 2004. Zircon (U–Th)/He thermochronometry: He diffusion and comparisons with $^{40}Ar/^{39}Ar$ dating. *Geochimica et Cosmochimica Acta*, **68**, 1857–1887.

Rosenberg, C. 2004. Shear zones and magma ascent: a model based on a review of the Tertiary magmatism in the Alps. *Tectonics*, **23**, TC3002.

Royden, L. & Horváth, F. (eds) 1988. *The Pannonian Basin: a Study in Basin Evolution*. *American Association of Petroleum Geologists, Memoir*s, **45**, 27–48.

Schefer, S., Cvetković, V., Fügenschuh, B., Kounov, A., Ovtcharova, M., Schaltegger, U. & Schmid, S. M., 2011. Cenozoic granitoids in the Dinarides of southern Serbia: age of intrusion, isotope geochemistry, exhumation history and significance for the geodynamic evolution of the Balkan Peninsula. *International Journal of Earth Sciences*, **100**, 1181–1206.

Shuster, D.L., Flowers, R.M. & Farley, K.A. 2006. The influence of natural radiation damage on helium diffusion kinetics in apatite. *Earth and Planetary Science Letters*, **249**, 148–161.

Sláma, J., Košler, J. *et al.* 2008. Plešovice zircon — a new natural reference material for U–Pb and Hf isotopic microanalysis. *Chemical Geology*, **249**, 1–35.

Stockli, D.F., Farley, K.A. & Dumitru, T.A. 2000. Calibration of the apatite (U–Th)/He thermochronometer on an exhumed fault block, White Mountains, California. *Geology*, **28**, 983–986.

Szabó, C., Harangi, S. & Csontos, L. 1992. Review of Neogene and Quaternary volcanism of the Carpathian-Pannonian region. *Tectonophysics*, **208**, 243–256.

Szádeczky-Kardoss, E. 1958. A vulkani hegysegek kutatasanak nehany alapkerdeserol. *Földtani Közlöny (Bulletin of the Hungarian Geological Society)*, **88**, 171–200.

Székyné, F.V. 1957. Some comments on the Tertiary volcanic activity on Transdanubia. *Földtani Közlöny (Bulletin of the Hungarian Geological Society)*, **87**, 63–68.

Takács, Á, Molnár, F., Turi, J., Mogessie, A. & Menzies, J.C. 2017. Ore mineralogy and fluid inclusion constraints on the temporal and spatial evolution of a high-sulfidation epithermal Cu-Au-Ag deposit in the Recsk ore complex, Hungary. *Economic Geology*, **112**, 1461–1481.

Tari, G., Báldi, T. & Báldi-Beke, M. 1993. Paleogene retroarc flexural basin beneath the Neogene Pannonian Basin: a geodynamic model. *Tectonophysics*, **226**, 433–455.

Varga, G., Csillag-Teplánszky, E. & Félegyházi, Z. 1975. *Geology of the Mátra Mountains*. Műszaki könyvkiadó, Budapest [*in Hungarian]*.

von Blanckenburg, F. & Davies, J.H. 1995. Slab breakoff: a model for syncollisional magmatism and tectonics in the Alps. *Tectonics*, **14**, 120–131.

Wagner, G. 1979. *Correction and interpretation of fission track ages. In*: Jäger, E. & Hunziker, J.C. (eds) Lectures in Isotope Geology. Springer, Berlin, 170–177.

Wiedenbeck, M., Alle, P. *et al.* 1995. Three natural zircon standards for U-Th-Pb, Lu-Hf, trace element and REE analyses. *Geostandards and Geoanalytical Research*, **19**, 1–23.

Zeitler, P., Herczeg, A., McDougall, I. & Honda, M. 1987. U–Th-He dating of apatite: a potential thermochronometer. *Geochimica et Cosmochimica Acta*, **51**, 2865–2868.

Zelenka, T. 2010. The Palaeogene and Neogene volcanism of the Mátra Mountains. *In:* C. Baráz (ed) *A Mátrai Tájvédelmi Körzet - Heves és Nógrád határán [The Mátra Landscape Park at the Border of Nógrád and Heves Counties]*. Publications of the Bükk National Park, Eger, 27–38 [in Hungarian].

Zelenka, T., Pécskay, Z., Kiss, J. & Szakács, A. 2004. New data on stratigraphic position of the Tar Dacite Tuff Formation, Hungary [in Hungarian with English abstract]. *A Magyar Állami Földtani Intézet Éves Jelentése*, **86**, 73–85.